

V.R. Shaginyan · V.A. Stephanovich · A.Z.
Msezane · P. Schuck · J.W. Clark · M. Ya.
Amusia · G.S. Japaridze · K.G.Popov · E.V.
Kirichenko

New state of matter: heavy-fermion systems, quantum spin liquids, quasicrystals, cold gases, and high temperature superconductors

the date of receipt and acceptance should be inserted later

Abstract We report on a new state of matter manifested by strongly correlated Fermi systems including various heavy-fermion (HF) metals, two-dimensional quantum liquids such as ^3He films, certain quasicrystals, and systems behaving as quantum spin liquids. Generically, these systems can be viewed as HF systems or HF compounds, in that they exhibit typical behavior of HF metals. At

V.R. Shaginyan
Petersburg Nuclear Physics Institute of NRC "Kurchatov Institute";
Gatchina, 188300, Russia,
CTSPS, Clark Atlanta University,
Atlanta, Georgia 30314, USA
E-mail: vrshag@thd.pnpi.spb.ru
V.A. Stephanovich
Institute of Physics, Opole University,
Oleska 48, 45-052, Opole, Poland
E-mail: stef@uni.opole.pl
A.Z. Msezane
CTSPS, Clark Atlanta University,
Atlanta, Georgia 30314, USA
P.Schuck
Institut de Physique Nucléaire, IN2P3-CNRS, Université Paris-Sud, F-91406 Orsay Cedex,
France
J.W. Clark
McDonnell Center for the Space Sciences & Department of Physics, Washington University,
St. Louis, MO 63130, USA; Center for Mathematical Sciences, University of Madeira, Funchal,
9000-390 Portugal
M. Ya. Amusia
Racah Institute of Physics, Hebrew University, Jerusalem 91904, Israel,
Ioffe Physical Technical Institute, RAS, St. Petersburg 194021, Russia
G. S. Japaridze
Clark Atlanta University, Atlanta, GA 30314, USA
K.G.Popov
Komi Science Center, Ural Division, RAS, 3a, Chernova str. Syktyvkar, 167982, Russia
E.V. Kirichenko
Institute of Mathematics and Informatics, Opole University, Oleska 48, 45-052, Opole, Poland

zero temperature, such systems can experience a so-called fermion-condensation quantum phase transition (FCQPT). Combining analytical considerations with arguments based entirely on experimental grounds we argue and demonstrate that the class of HF systems is characterized by universal scaling behavior of their thermodynamic, transport, and relaxation properties. That is, the quantum physics of different HF compounds is found to be universal, emerging irrespective of the individual details of their symmetries, interactions, and microscopic structure. This observed universal behavior reveals the existence of a new state of matter manifest in HF compounds. We propose a simple, realistic model to study the appearance of flat bands in two-dimensional ensembles of ultracold fermionic atoms, interacting with coherent resonant light. It is shown that signatures of these flat bands may be found in peculiarities in their thermodynamic and spectroscopic properties. We also show that the FCQPT, in generating flat bands and altering Fermi surface topology, is an essential progenitor of the exotic behavior of the overdoped high-temperature superconductors represented by $\text{La}_{2-x}\text{Sr}_x\text{CuO}_4$, whose superconductivity differs from that predicted by the classical Bardeen-Cooper-Schrieffer theory. The theoretical results presented are in good agreement with recent experimental observations, closing the colossal gap between these empirical findings and Bardeen-Cooper-Schrieffer-like theories.

Keywords quantum phase transition, flat bands, high- T_c superconductivity, non-Fermi-liquid states, strongly correlated electron systems, cold gases, quantum spin liquids, heavy fermions, quasicrystals, new state of matter

1 Introduction

Strongly correlated Fermi systems, such as heavy fermion (HF) metals, high- T_c superconductors, two-dimensional liquids like ^3He , compounds with quantum spin liquids, quasicrystals, and systems with one-dimensional quantum spin liquid, are among the most intriguing and thoroughly experimentally studied fundamental systems in physics. The properties of these materials, called HF compounds, differ dramatically from those of ordinary systems of interacting fermions, well described within the framework of famous Landau Fermi liquid (LFL) theory, see e.g. [1–18]. For instance, in the case of metals with HF, the strong electron-electron correlations lead to renormalization of the quasiparticles effective mass M^* , which may exceed the ordinary, "bare", mass by several orders of magnitude or even become infinitely large. The effective mass strongly depends on the temperature, pressure, or applied magnetic field. Such metals exhibit NFL behavior and unusual power laws of the temperature dependence of the thermodynamic properties at low temperatures.

The Landau theory of the Fermi liquid is based on the mapping of the system (liquid) of strongly interacting electrons and nuclei to that of a weakly interacting Fermi gas. This implies that the elementary excitations behave as quasiparticles of a weakly interacting Fermi gas, determining the system physical properties at low temperatures. Thus latter excitations have a certain effective mass M^* , which depends weakly on temperature, pressure, and magnetic field strength, and is a parameter of the theory [19–21]. The LFL theory fails to explain the results of experimental observations related to the dependence of M^* on the temperature

T , magnetic field B , pressure and other external stimuli. This led to the evasive conclusion that quasiparticles do not survive in strongly correlated Fermi systems and that the heavy electron does not retain its identity as a quasiparticle excitation [7–13, 18].

The unusual properties and NFL behavior observed in HF compounds are assumed to be determined by various magnetic quantum phase transitions [1–9, 11–14]. Since a quantum phase transition occurs at the temperature $T = 0$, the control parameters are the composition, electron (hole) number density x , pressure, magnetic field strength B , etc. A quantum phase transition occurs at a quantum critical point, which separates the ordered phase that emerges as a result of quantum phase transition from the disordered phase. It is usually assumed that magnetic (e.g., ferromagnetic and antiferromagnetic) quantum phase transitions are responsible for the NFL behavior. The critical point of such a phase transition can be shifted to absolute zero by varying the above parameters. The observed universal behavior can be expected only if the system under consideration is very close to a quantum critical point, e.g., when the correlation length is much longer than the microscopic length scale, and critical quantum and thermal fluctuations determine the anomalous contribution to the thermodynamic functions of the metal. Quantum phase transitions of this type are so widespread [2–4, 9–13] that we call them ordinary quantum phase transitions [22–24]. In this case, the physics of the phenomenon is determined by thermal and quantum fluctuations of the critical state, while quasiparticle excitations are destroyed by these fluctuations. Conventional arguments that quasiparticles in strongly correlated Fermi liquids "get heavy and die" at a quantum critical point commonly employ the well-known formula based on the assumptions that the z -factor (the quasiparticle weight in the single-particle state) vanishes at the points of second-order phase transitions [18]. However, it has been shown that this scenario is problematic [23–26], while in the case of the heavy-fermion (HF) metal β – YbAlB₄ experimental facts show that magnetic quantum phase transitions and the corresponding fluctuations are not responsible for the observed NFL behavior [23, 24, 27, 28]. The same conclusion is true in the case of compounds with strongly correlated quantum spin liquids, two-dimensional liquids like ³He, quasicrystals, and systems with one-dimensional quantum spin liquid [29–35].

Another difficulty is in explaining the restoration of the LFL behavior under the application of magnetic field B , as observed in HF metals and in high- T_c superconductors [1, 15, 36] and the other HF compounds, see Section 3. For the LFL state as $T \rightarrow 0$, the electric resistivity $\rho(T) = \rho_0 + AT^2$, the heat capacity $C(T) = \gamma_0 T$, and the magnetic susceptibility $\chi = const$. It turns out that the coefficient $A(B)$, the Sommerfeld coefficient $\gamma_0(B) \propto M^*$, and the magnetic susceptibility $\chi(B)$ depend on the magnetic field strength B such that $A(B) \propto \gamma_0^2(B)$ and $\chi(B) \propto \chi^2(B)$, which implies that the Kadowaki-Woods relation $K = A(B)/\gamma_0^2(B)$ [37] is B -independent and is preserved [15]. Such universal behavior, quite natural when quasiparticles with the effective mass M^* playing the main role, can hardly be explained within the framework of the approach that presupposes the absence of quasiparticles, which is characteristic of ordinary quantum phase transitions in the vicinity of QCP. Indeed, there is no reason to expect that γ_0 , χ and A are affected by the fluctuations in a correlated fashion. For instance, the Kadowaki-Woods relation does not agree with the spin density wave scenario [15] and with

the results of research in quantum criticality based on the renormalization-group approach [38]. Moreover, measurements of charge and heat transfer have shown that the Wiedemann-Franz law holds in some high- T_c superconductors [36, 39] and HF metals [40–43]. All this suggests that quasiparticles do exist in HF compounds, and this conclusion is also corroborated by photoemission spectroscopy results and measurements of the Kadowaki-Woods relation in such uncommon HF compound as quasicrystals, see e.g. [44–46]. We show that the basic properties of HF compounds can be described within the framework of a fermion condensation quantum phase transition (FCQPT), leading to formation of fermion condensation (FC) and flat bands, and extended quasiparticle paradigm that allow us to explain the non-Fermi liquid behavior observed in strongly correlated Fermi systems [23, 24]. In contrast to the Landau paradigm assuming that the quasiparticle effective mass is approximately constant, the effective mass of new quasiparticles strongly depends on temperature, magnetic field, pressure, and other parameters. We note that the direct experimental manifestation of FC has been done recently [47].

The rest of the paper is organized as follows: In Section 2, we use HF metals as an example, and outline the scaling behavior observed in HF compounds. Upon introducing internal scales, we show that the behavior is universal for HF compounds. In Sections 3 we examine the universal scaling behavior of the thermodynamic, transport and relaxation properties of HF compounds magnets of new types with strongly correlated quantum spin liquid (SCQSL), the recently discovered quasicrystals, respectively, and show that these HF compounds demonstrate the new state of matter. Section 4 presents a perspective simple realistic model to observe the appearance of flat bands in two-dimensional ensemble of ultracold fermionic atoms, interacting with coherent resonant light. In Section 5, we show that FCQPT, generating flat bands and altering Fermi surface topology, is a primary reason for the recently observed behavior of the overdoped high-temperature superconductors represented by $\text{La}_{2-x}\text{Sr}_x\text{CuO}_4$, whose superconductivity features differ from what is predicted by the classical Bardeen-Cooper-Schrieffer theory. Section 6 summaries the main results, stressing the observation that the quantum physics of different HF compounds is universal and emerges regardless of their underlying microscopic details. This uniform behavior, formed by flat bands, manifests the new state of matter.

2 Scaling behavior and internal scales

As we have mentioned in Section 1, the NFL behavior manifests itself in the power-law behavior of the physical quantities of HF compounds, with exponents different from those of a Fermi liquid [50, 51]. It is common belief that the main output of theory is the explanation of these exponents which are at least depended on the magnetic character of QCP and dimensionality of the system. On the other hand, the NFL behavior cannot be captured by these exponents as seen from Fig. 1. Indeed, as a function of T at fixed B , the specific heat C/T exhibits a behavior that is to be described as a function of both temperature T and magnetic B field rather than by a single exponent. One can see that at low temperatures C/T demonstrates the LFL behavior which is changed by the transition regime at which C/T reaches its maximum and finally C/T decays into NFL behavior. It is seen

from Fig. 1 that, both being checked in the LFL regime and in the transition one, these exponents may have little physical significance.

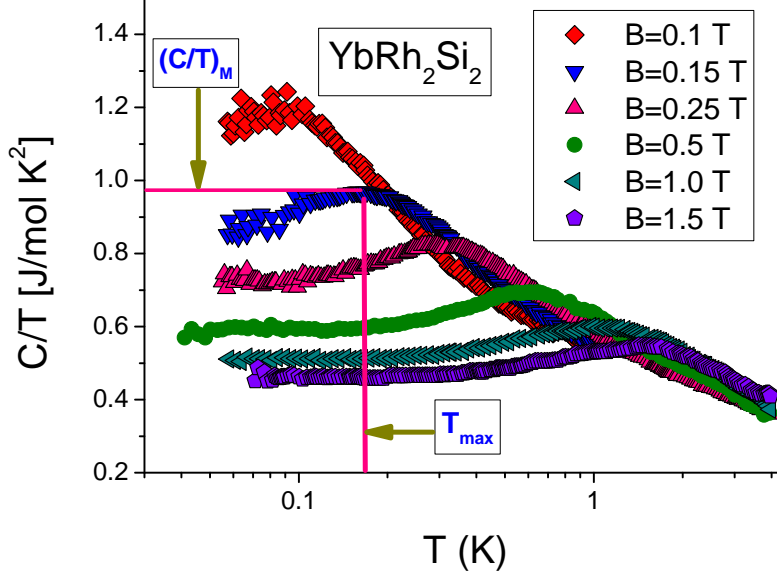


Fig. 1 (Color online) Electronic specific heat of YbRh_2Si_2 , C/T , versus temperature T as a function of magnetic field B [50] shown in the legend.

In order to reveal the universal scaling behavior, and to establish that salient properties of C/T displayed in Fig. 1 possess generic character, we recall that can be helpful to use “internal” scales to measure the effective mass $M^* \propto C/T$ and temperature T [23, 24, 52, 53]. As successively higher magnetic fields are applied to the sample, Fig. 1 shows successive maxima $(C/T)_M$ in C/T at corresponding temperatures T_M , with T_M shifting to higher T as B is increased. The value of the Sommerfeld coefficient $C/T = \gamma_0$ is saturated towards lower temperatures, decreasing at elevated magnetic fields. To reveal a remarkable universal scaling behavior that is present independently of “incidental” system properties, we may adopt $(C/T)_M$ and T_M as relevant internal scales. Accordingly, the maximum structure $(C/T)_M$ in C/T is used to normalize C/T , while T is normalized by T_M . The resulting plots of the normalized $(C/T)_N = (C/T)/(C/T)_M$ versus the normalized temperature variable $y = T_N = T/T_M$ fields are displayed in Fig. 2. The normalized experimental results for the different magnetic fields B are seen to merge into a single curve over an extended range in y , providing clear documentation of universal scaling behavior, with LFL and NFL regimes separated by a transition region in which $(C/T)_N$ attains its maximum value.

To analyze dependence of the effective mass M^* on temperature T , magnetic field B , momentum p , number density x etc., we use the Landau equation for the

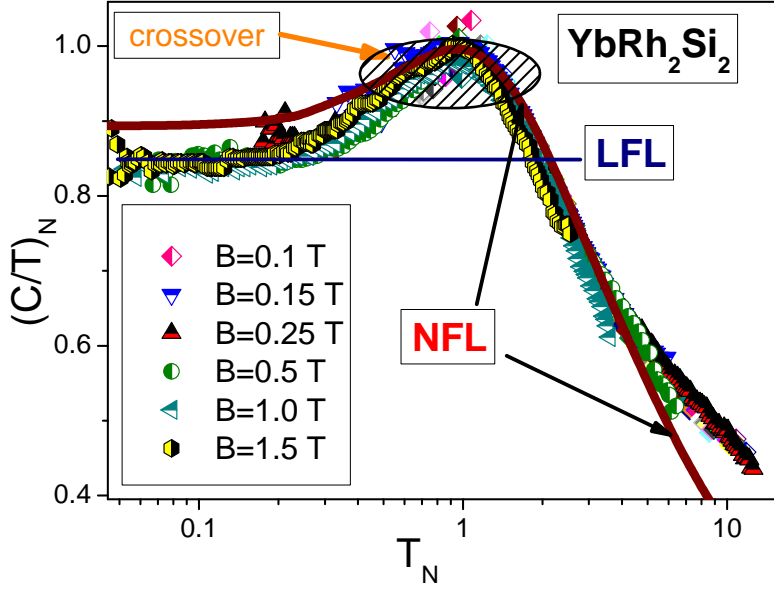


Fig. 2 (Color online) The normalized effective mass M_N^* versus normalized temperature T_N . M_N^* is extracted from the measurements of the specific heat C/T on YbRh_2Si_2 in magnetic fields B [50] listed in the legend. Constant effective mass inherent in normal Landau Fermi liquids is depicted by the solid line. The NFL regime is shown by the arrows. The crossover is depicted by the shaded area. The solid curve represents our calculation of the universal behavior of $(C/T)_N$.

effective mass M^* [19–21]

$$\frac{1}{M^*(T, B)} = \frac{1}{M} + \int \frac{\mathbf{p}_F \mathbf{p}_1}{p_F^3} F(\mathbf{p}_F, \mathbf{p}_1, n) \frac{\partial n(p_1, T, B)}{\partial p_1} \frac{d\mathbf{p}_1}{(2\pi)^3}, \quad (1)$$

expressed in terms of the bare mass M , the Landau interaction F , and the Fermi-Dirac distribution

$$n_{\pm}(p, T, B) = \left\{ 1 + \exp \left[\frac{\varepsilon(p, T) \pm B\mu_B - \mu}{T} \right] \right\}^{-1}. \quad (2)$$

Here, $n_{\pm}(p, T)$ and $\varepsilon(p, T)$ are respectively the the quasiparticle momentum distribution and ε the quasiparticle energy, with μ the chemical potential and μ_B the Bohr magneton. The term $\pm B\mu_B$ entering the right side of Eq. (2) describes the Zeeman splitting. Equation (1) is exact and can be derived within the framework of the Density Functional Theory [23, 24]. This equation allows us to calculate the behavior of M^* which now becomes a function of temperature T , external magnetic field B , number density x , pressure P , etc. Near FCQPT the normalized solution of Eq. (1) $M_N^*(T_N)$ can be approximated well by a simple universal interpolating function [23, 24]. The interpolation occurs between the LFL and NFL

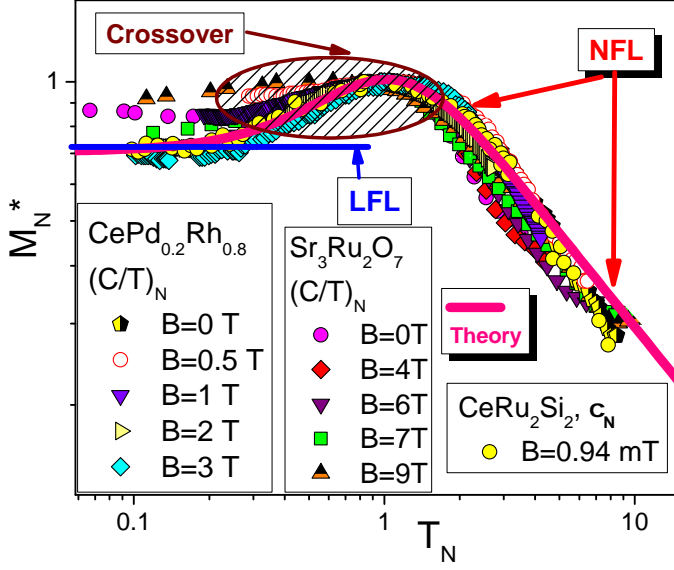


Fig. 3 The universal scaling behavior of the normalized effective mass M_N^* versus T_N , extracted from the measurements of χ and C/T , see Eq. (5), (in magnetic fields B shown in the legends) on CeRu_2Si_2 [54], $\text{CePd}_{1-x}\text{Rh}_x$ with $x = 0.80$ [51], and $\text{Sr}_3\text{Ru}_2\text{O}_7$ [55]. The LFL and NFL regimes are shown by the arrows. The crossover is depicted by the shaded area. The solid curve represents our calculation of the universal behavior of $M_N^*(T_N)$, see Eq. (3).

regimes and represents the universal scaling behavior of M_N^*

$$M_N^*(T_N) \approx c_0 \frac{1 + c_1 T_N^2}{1 + c_2 T_N^n}. \quad (3)$$

Here, $c_0 = (1 + c_2)/(1 + c_1)$, c_1 , c_2 are fitting parameters; and the exponent $n = 8/3$ if the Landau interaction is an analytical function, otherwise $n = 5/2$. It follows from Eq. (1) that

$$T_M \simeq a_1 \mu_B B, \quad (4)$$

where a_1 is a dimensionless number. The result (4) is in good agreement with experiment, although possible corrections to it near the corresponding phase transitions are discussed in Refs. [23, 24]. Importantly, the effective mass M^* defines the thermodynamic properties of HF compounds; schematically, $M^*(T) \propto C(T)/T \propto S(T)/T \propto \chi(T)$, where $C(T)$ is the specific heat, $S(T)$ the entropy, $M_0(T)$ the magnetization, and $\chi(T)$ the AC magnetic susceptibility. For the normalized values one has

$$M_N^* = (C/T)_N = (S/T)_N = \chi_N. \quad (5)$$

As seen from Fig. 2, the normalized effective mass $(C/T)_N = M_N^*(T_N)$ extracted from the measurements is not a constant, as would be for a LFL, and

shows the scaling behavior over three decades in normalized temperature T_N . It is seen from Figs. 1 and 2 that the NFL behavior and the associated scaling extend at least to temperatures up to few Kelvins. Scenario where fluctuations in the order parameter of an infinite (or sufficiently large) correlation length and an infinite correlation time (or sufficiently large) develop the NFL behavior can hardly match up such high temperatures, while the existence of quasiparticles completely account for this behavior [23, 24, 48, 49].

We are led to conclude that a central challenge for mechanistic theories of the critical behavior of the HF compounds, including HF metals, lies in explanation of the scaling behavior of $M_N^*(T_N)$. Theories calculating only the exponents characterizing $M_N^*(T_N)$ at $T_N \gg 1$ deal only with a part of the observations and overlook, for example, what is happening in the transition regime. Another qualitative aspect the problem calling for explanation is the remarkably large temperature ranges over which the NFL behavior is found to occur. Fig. 3 informs us that this key feature may in fact be understood within the theoretical framework of the fermion condensate (FC).

The behavior of the normalized effective mass extracted from measurements of χ and (C/T) in the compounds CeRu_2Si_2 [54], $\text{CePd}_{0.8}\text{Rh}_{0.8}$ [51], and $\text{Sr}_3\text{Ru}_2\text{O}_7$ [55] is displayed in Fig. 3. This figure shows the main features of the scaling behavior of the normalized effective mass M_N^* as given by Eq. (3). At low temperatures $T_N < 1$ the normalized effective mass is in the LFL domain; with rising T_N it crosses over through the transition, finally entering the NFL regime. The solid curve is the result of our calculation of the scaling behavior. It is seen that $\text{Sr}_3\text{Ru}_2\text{O}_7$, located at the metamagnetic transition, and the two HF metals exhibit the same scaling behavior, which is common to other HF compounds and which can be understood within the framework of fermion condensation or flat-band theory [23, 24, 48, 49, 56]. As we will be emphasized below, large temperature ranges are symptomatic of new quasiparticles, and it is the scaling behavior of the normalized effective mass that allows us to explain different properties of HF compounds in their LFL, crossover, and NFL regimes and to demonstrate that HF compounds, expressing universal scaling behavior, represent a new state of matter.

3 Strongly correlated quantum spin liquids and quasicrystals

3.1 Introduction

In a frustrated magnet, spins are prevented from forming an ordered alignment, so even at temperatures close to absolute zero they collapse into a liquid-like state called a quantum spin liquid (QSL). The herbertsmithite $\text{ZnCu}_3(\text{OH})_6\text{Cl}_2$ has been exposed as a $S = 1/2$ kagome antiferromagnet [57], and recent experimental investigations have revealed its unusual behavior [58–60]. Because of its electrostatic environment, Cu^{2+} is expected to occupy the distorted octahedral kagome sites. Magnetic kagome planes Cu^{2+} $S = 1/2$ are separated by nonmagnetic Zn^{2+} layers. Observations have found no evidence of long-range magnetic order or spin freezing down to temperature of 50 mK, indicating that $\text{ZnCu}_3(\text{OH})_6\text{Cl}_2$ is the best model found of the quantum kagome lattice [58–60]. These results are confirmed by theoretical considerations demonstrating that the ground state of kagome antiferromagnet is a gapless spin liquid [30–32, 61]. On the other hand, it

has recently been suggested that there exists a small spin-gap in the kagome layers [62–64]. The results reported are based on both experimental facts and theoretical interpretation of these results within the framework of impurity model. The experimental facts are derived from high-resolution low-energy inelastic neutron scattering on single-crystal $\text{ZnCu}_3(\text{OH})_6\text{Cl}_2$ Herbertsmithite, with the prospect of disentangling the effects on the observed properties of this material due to Cu impurity spins from the effects of the kagome lattice itself [62]. The impurity model assumes that the corresponding impurity system may be represented as a simple cubic lattice in the dilute limit below the percolation threshold. The model then suggests that the spin gap survives under the application of magnetic fields up to 9 T [64], while in the absence of magnetic fields the bulk spin susceptibility χ exhibits a divergent Curie-like tail, indicating that some of the Cu spins act like weakly coupled impurities [62–64]. We will argue that the proposed impurity model is artificial because it is impossible to isolate the contributions coming from the impurities and the kagome planes, in that the impurities and the kagome planes should be considered as an integral system. The model is therefore inconsistent with the intrinsic properties of $\text{ZnCu}_3(\text{OH})_6\text{Cl}_2$ as observed and described in recent experimental and theoretical studies of the behavior of its thermodynamic, dynamic, and relaxation properties. We demonstrate that explanation of these properties lies in the physics of the strongly correlated quantum spin liquid (SCQSL) present in this system, for the behavior of $\text{ZnCu}_3(\text{OH})_6\text{Cl}_2$ is in fact similar to that of heavy-fermion metals and quasicrystals, with one main exception — $\text{ZnCu}_3(\text{OH})_6\text{Cl}_2$ does not support an electrical current [23, 24, 30–32, 34, 65–67]. We conclude by outlining a program to clarify the existence of SCQSL. In particular, we suggest that measurements of heat transport and inelastic neutron scattering in magnetic fields B be carried out. Such measurements could be crucial in revealing both the mechanisms involved and the real physics of QSL in $\text{ZnCu}_3(\text{OH})_6\text{Cl}_2$.

3.2 Thermodynamic properties

To examine the impurity model in a broader context, we first refer to the experimental behavior of the magnetic susceptibility χ of Herbertsmithite. It is seen from Fig. 4 that the magnetic susceptibility has the divergent behavior $\chi(T) \propto T^{-2/3}$, in magnetic fields $B \leq 1$ T, as shown by the solid line. In the case of weakly interacting impurities it is suggested that the low-temperature behavior of $\chi_{\text{CW}}(T) \propto 1/(T + \theta)$ can be approximated by a Curie-Weiss law [62–64], with θ a vanishingly small Weiss temperature. However, given that $\chi(T) \propto T^{-2/3}$, the Curie-Weiss approximation is in conflict with both experiment [58] and theory [24, 30]. Within the framework of the impurity model, the calculated intrinsic spin susceptibility of the kagome plane obeys $\chi_{\text{kag}}(T) = \chi(T) - \chi_{\text{CW}}(T)$, leading to $\chi_{\text{kag}}(T \rightarrow 0) \rightarrow 0$ and the erroneous claim that a putative gap has been observed [63]. Thus, we must conclude that the impurity model is not valid, since it cannot explain the empirically validated behavior $\chi(T) \propto T^{-2/3}$. To explain this behavior of χ , it is necessary to consider the impurities and the kagome planes as an integral system [23, 24, 30–32, 34, 65–67].

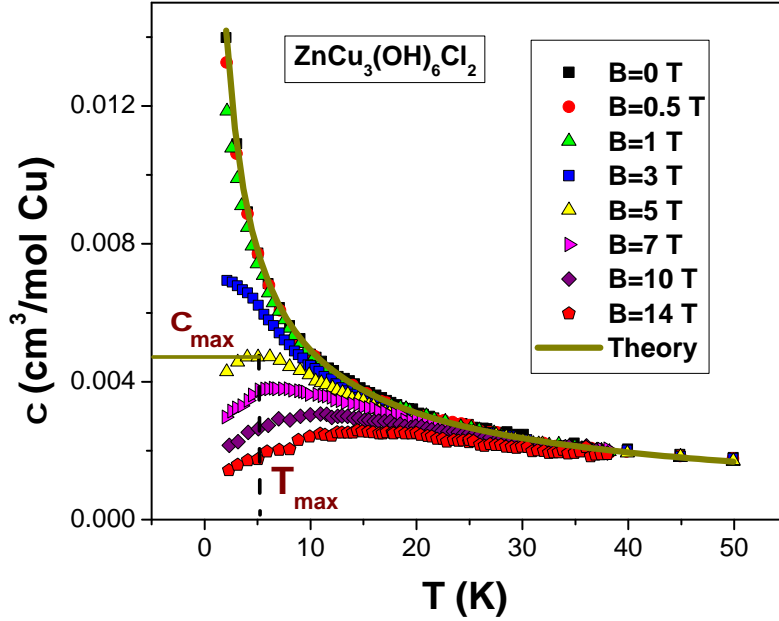


Fig. 4 (Color online) Measured temperature dependence of the magnetic susceptibility χ of $\text{ZnCu}_3(\text{OH})_6\text{Cl}_2$ from Ref. [58] at magnetic fields shown in the legend. Illustrative values of χ_{max} and T_{max} at $B = 3$ T are also shown. A theoretical prediction at $B = 0$ is plotted as the solid curve, which represents $\chi(T) \propto T^{-\alpha}$ with $\alpha = 2/3$ [24, 30].

In similar vein, working within the impurity model the authors of Ref. [62] obtain a measure $S_{\text{kag}}(\omega) = S_{\text{tot}}(\omega) - aS_{\text{imp}}(\omega)$ of the intrinsic scattering by subtracting the impurity scattering $S_{\text{imp}}(\omega)$ from the total scattering $S_{\text{tot}}(\omega)$, taking a as a fitting parameter. As a result, they find that $S_{\text{kag}}(\omega) \rightarrow 0$ as ω decreases below an energy of 0.7 meV (see Fig. 4(b) of Ref. [62]) and claim observation of a gap, whereas we have shown above that such a subtraction leads to the erroneous conclusion that a gap has been found. Indeed, this conclusion relies completely on the theoretical assumption that the impurities are weakly interacting; accordingly, it cannot be considered as experimental fact.

Let us consider somewhat further the inadequacy of the impurity model and its corresponding gap, when confronted with experimental findings. We see from Fig. 4 that Landau Fermi liquid (LFL) behavior is demonstrated at least for $B \geq 3$ T and low temperatures T . At such temperatures and magnetic fields the impurities should become fully polarized. They do not exhibit typical Curie-Weiss behavior; otherwise the impurity mode would fail. Thus, assuming the impurities are fully polarized and hence do not contribute to χ , one has simply $\chi_{\text{kag}}(T) = \chi(T)$. Analogous behavior for the heat capacity follows from Fig. 5. LFL behavior of C_{mag}/T emerges under application of the same fields. Consequently, we may conclude that at least at $B \geq 3$ T and low T , the contributions to both χ and C_{mag}/T from the impurities are negligible; rather, one expects them to be dominated by

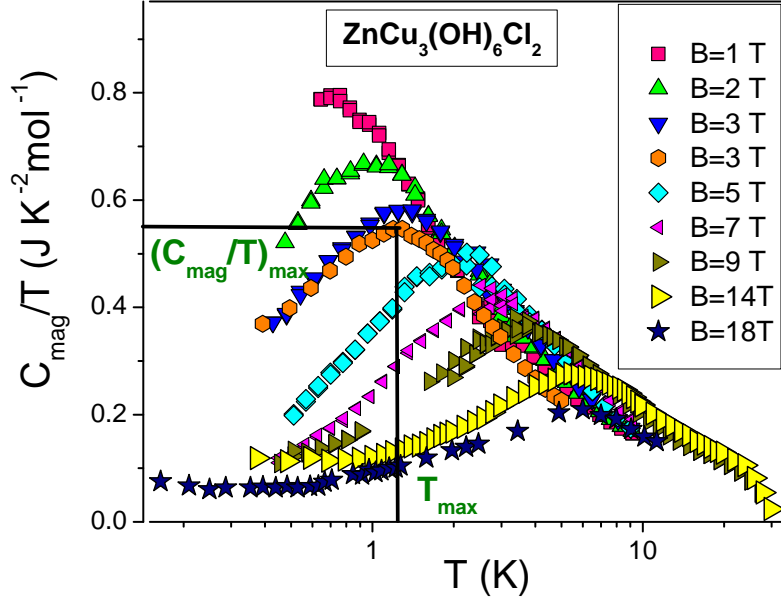


Fig. 5 (Color online) Specific heat C_{mag}/T measured on powder [59, 60] and single-crystal [57, 68, 69] samples of Herbertsmithite is displayed as a function of temperature T for fields B shown in the legend.

the kagome lattice, exhibiting a spin gap in the kagome layers [62–64]. Thus, according to the impurity model one would expect both $\chi(T)$ and $C_{\text{mag}}(T)/T$ to approach zero for $T \rightarrow 0$ at $B \geq 3$ T. From Figs. 4, 5, and 6, it is clear that this is not the case. Up to $B \sim 14$ T neither χ nor C_{mag}/T approaches zero as $T \rightarrow 0$. Moreover, the normalized C_{mag}/T follows the uniform scaling behavior displayed in Fig. 6, confirming the absence of a gap. Also, as indicated in Fig. 5, it is found that the recent measurements of C_{mag} [57, 59, 60, 68, 69] are compatible with those obtained on powder samples. All relevant experimental observations support the conclusions that (i) the properties of $\text{ZnCu}_3(\text{OH})_6\text{Cl}_2$ under study are determined by a stable SCQSL, (ii) there is no appreciable gap in the spectra of spinon excitations, such a gap being absent even under the application of very high magnetic fields of 18 T, and (iii) the impurity model is untenable from the experimental standpoint. These conclusions agree with recent experimental findings that the low-temperature plateau in local susceptibility identifies the spin-liquid ground state as being gapless [70], while recent theoretical analysis confirms the absence of a gap [61].

3.3 Relaxation and transport properties

The same conclusions can be drawn from the results of neutron-scattering measurements of the dynamic spin susceptibility $\chi(\mathbf{q}, \omega, T) = \chi'(\mathbf{q}, \omega, T) + i\chi''(\mathbf{q}, \omega, T)$

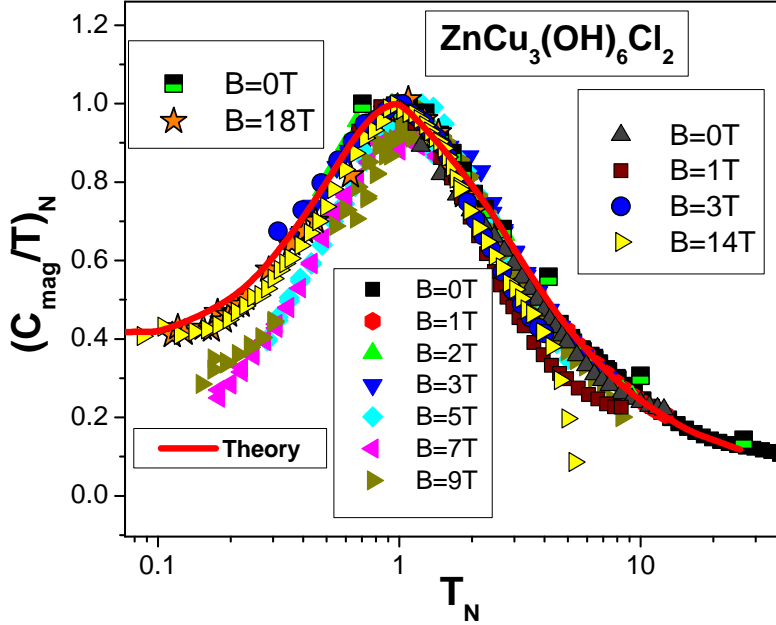


Fig. 6 (Color online) Normalized specific heat $(C_{\text{mag}}/T)_N$ versus normalized temperature T_N at B -field values shown in the legend [24, 66]. The theoretical result from Refs. [24, 30], represented by the solid curve, traces the scaling behavior of the effective mass.

as a function of momentum q , frequency ω , and temperature T . Indeed, these results play a crucial role in identifying the properties of the quasiparticle excitations involved. At low temperatures, such measurements reveal that the corresponding quasiparticles – of a new type insulator – are represented by spinons, form a continuum, and populate an approximately flat band crossing the Fermi level [71]. In such a situation it is expected that the dimensionless normalized susceptibility $(T^{2/3}\chi'')_N = T^{2/3}\chi''/(T^{2/3}\chi'')_{\text{max}}$ exhibits scaling as a function of the dimensionless energy variable $E_N = E/E_{\text{max}}$ [24, 31]. Specifically, the equation describing the normalized susceptibility $(T^{2/3}\chi'')_N$ reads [24, 31]

$$(T^{2/3}\chi'')_N \simeq \frac{b_1 E_N}{1 + b_2 E_N^2}, \quad (6)$$

where b_1 and b_2 are fitting parameters adjusted such that the function $(T^{2/3}\chi'')_N$ reaches its maximum value unity at $E_N = 1$ [24, 31]. Figure 7 displays $(T^{2/3}\chi'')_N$ values extracted from measurements of the inelastic neutron-scattering spectrum on the heavy-fermion (HF) metal $\text{Ce}_{0.925}\text{La}_{0.075}\text{Ru}_2\text{Si}_2$ [72]. The scaled data for this quantity, obtained from measurements on two quite different strongly correlated systems, $\text{ZnCu}_3(\text{OH})_6\text{Cl}_2$ [58] and $(\text{D}_3\text{O})\text{Fe}_3(\text{SO}_4)_2(\text{OD})_6$ [73], are displayed in Figs. 8 and 9, respectively. It is seen that the theoretical results from

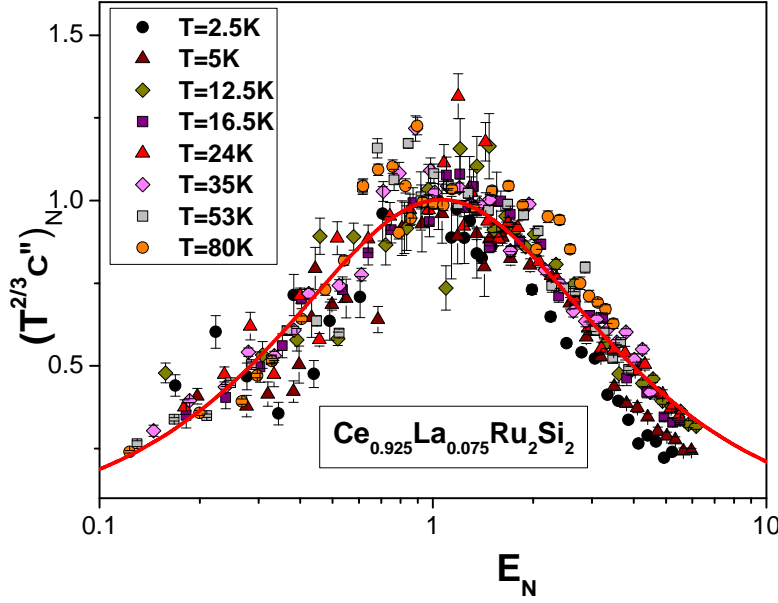


Fig. 7 (Color online) Scaling behavior of the normalized dynamic spin susceptibility $(T^{2/3}\chi'')_N$. Data are extracted from measurements on the heavy-fermion metal $\text{Ce}_{0.925}\text{La}_{0.075}\text{Ru}_2\text{Si}_2$ [72] and plotted against the dimensionless variable E_N . Solid curve: Theoretical calculations based on Eq. (6) [31].

Ref. [31] (solid curves) are in good agreement with the experimental data collected on all three compounds over almost three orders of magnitude of the scaled variable E_N . Hence $(T^{2/3}\chi'')_N$ does exhibit the anticipated scaling behavior for these systems. From this observation we infer that the spin excitations in both $\text{ZnCu}_3(\text{OH})_6\text{Cl}_2$ and $(\text{D}_3\text{O})\text{Fe}_3(\text{SO}_4)_2(\text{OD})_6$ demonstrate the same itinerate behavior as the electronic excitations of the HF metal $\text{Ce}_{0.925}\text{La}_{0.075}\text{Ru}_2\text{Si}_2$ and therefore form a continuum. This detection of a continuum is of great importance since it clearly signals the presence of a SCQSL in Herbertsmithite [24, 31, 32].

Provided that a fermion condensate (FC) is indeed present in the electronic system of a HF metal, we know that the imaginary part $\chi''(T, \omega)$ of the susceptibility is given by [24, 74]

$$T\chi''(T, \omega) \simeq \frac{a_5 E}{1 + a_6 E^2}, \quad (7)$$

where $E = \omega/k_B T$ while a_5 and a_6 are constants. It is seen from Eq. (7) that $T\chi''(T, \omega)$ depends on the only the variable $E = \omega/k_B T$. Thus, Eqs. (6) and (7) establish two types of scaling behavior of $\chi''(\omega, T)$. In Fig. 10, the dynamic susceptibility $(T\chi'')$ extracted from measurements of the inelastic neutron scatter-

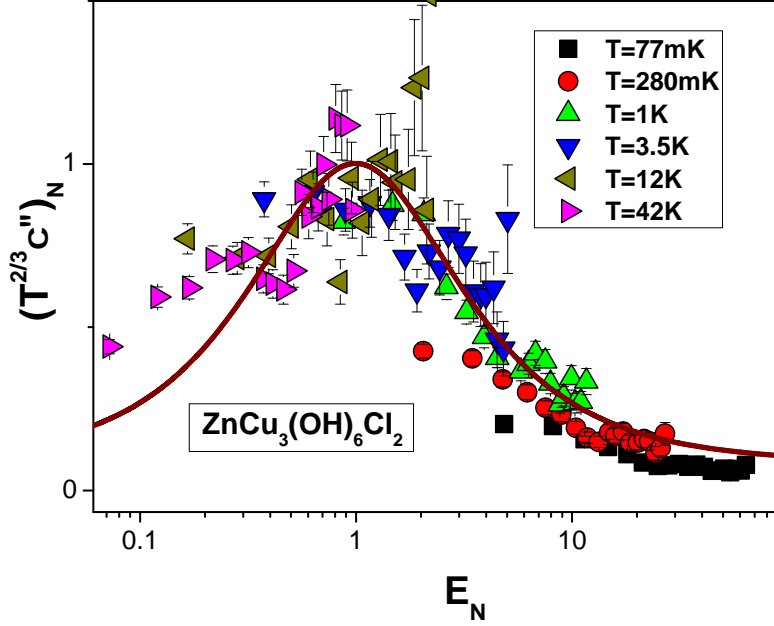


Fig. 8 (Color online) Scaling behavior of the normalized dynamic spin susceptibility $(T^{2/3}\chi'')_N$. Data are extracted from measurements on Herbertsmithite $\text{ZnCu}_3(\text{OH})_6\text{Cl}_2$ [58]. Solid curve: Theoretical calculations based on Eq. (6) [31].

ing spectrum on the HF metal YbRh_2Si_2 [75] is shown. The data for $(T\chi'')$ exhibit scaling behavior over three decades in the variation of both this function and the variable E , thus confirming the validity of Eq. (7). The scaled data obtained in measurements on such quite different strongly correlated systems as $\text{ZnCu}_3(\text{OH})_6\text{Cl}_2$, $\text{Ce}_{0.925}\text{La}_{0.075}\text{Ru}_2\text{Si}_2$, $(\text{D}_3\text{O})\text{Fe}_3(\text{SO}_4)_2(\text{OD})_6$, and YbRh_2Si_2 collapse fairly well onto a single curve over almost three decades of the scaled variables.

It is apparent from Figs. 7, 8, 9, and 10 that the calculations based on this premise are in good agreement with the experimental data, affirming the identification of SCQSL as the agent responsible for the low-temperature behavior of $\text{ZnCu}_3(\text{OH})_6\text{Cl}_2$ and $(\text{D}_3\text{O})\text{Fe}_3(\text{SO}_4)_2(\text{OD})_6$. We conclude that the concept of the spin gap in the kagome layers is an artificial construct at odds with known properties of $\text{ZnCu}_3(\text{OH})_6\text{Cl}_2$, thereby negating the existence of a spin gap in the SCQSL of Herbertsmithite. It is noted that the presence of a gap in the kagome layers is not in itself of vital importance, for it does not govern the thermodynamic and transport properties of $\text{ZnCu}_3(\text{OH})_6\text{Cl}_2$. Rather, these properties are determined by the underlying SCQSL. This assertion can be tested by measurements of the heat transport in magnetic fields, as has been done successfully in the case of the organic insulators $\text{EtMe}_3\text{Sb}[\text{Pd}(\text{dmit})_2]_2$ and $\kappa - (\text{BEDT} -$

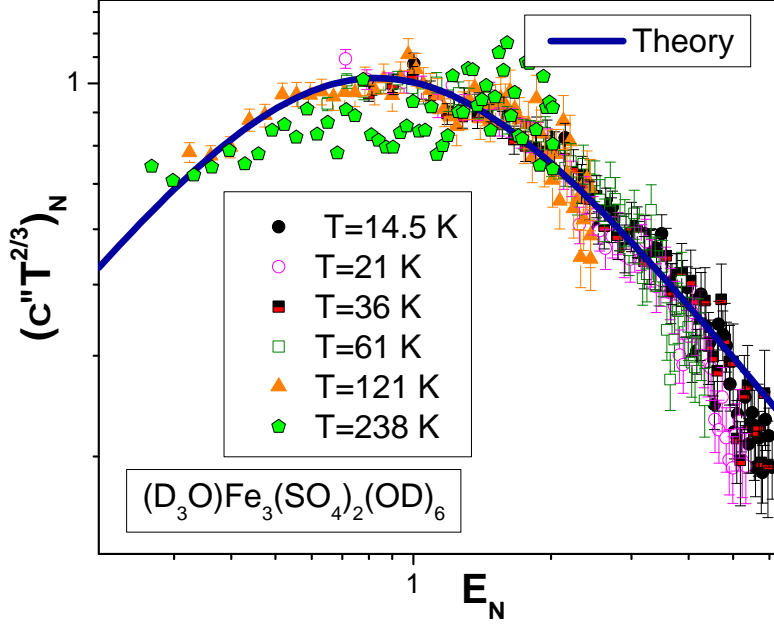


Fig. 9 (Color online) Scaling behavior of the normalized dynamic spin susceptibility $(T^{2/3}\chi''_N)$. Data are extracted from measurements on the deuterium jarosite $(D_3O)Fe_3(SO_4)_2(OD)_6$ [73]. Solid curve reports the theoretical calculations based on Eq. (6) [31].

$TTF)_2Cu_2(CN)_3$ [65, 76, 77]. Measurements of thermal transport are particularly salient in that they probe the low-lying elementary excitations of SCQSL in $ZnCu_3(OH)_6Cl_2$ and potentially reveal itinerant spin excitations that are mainly responsible for the heat transport. Surely, the overall heat transport is contaminated by the phonon contribution; however, this contribution is hardly affected by the magnetic field B . Essentially, we expect that measurement of the B -dependence of thermal transport will be an important step toward resolving the nature of the SCQSL in $ZnCu_3(OH)_6Cl_2$ [24, 32, 65].

The SCQSL in Herbertsmithite behaves like the electron liquid in HF metals – provided the charge of an electron is set to zero. As a result, the thermal resistivity w of the SCQSL is given by [24, 32, 65]

$$w - w_0 = W_r T^2 \propto \rho - \rho_0 \propto (M^*)^2 T^2, \quad (8)$$

where $W_r T^2$ represents the contribution of spinon-spinon scattering to thermal transport, being analogous to the contribution AT^2 to charge transport from electron-electron scattering. Here ρ is the longitudinal magnetoresistivity (LMR), and w_0 and ρ_0 are the residual thermal resistivity and residual resistivity, respectively.

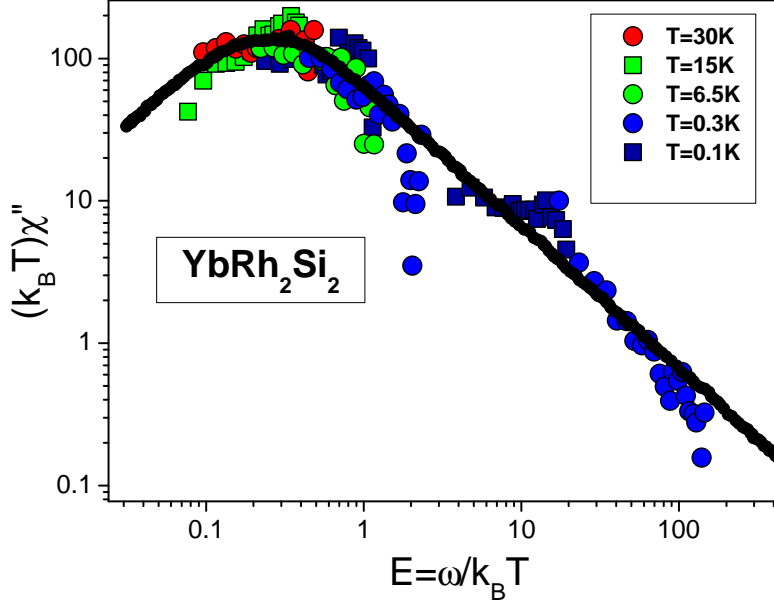


Fig. 10 (Color online) Scaling behavior of the normalized dynamic spin susceptibility $T\chi''$ plotted against $E = \omega/k_B T$. The data are extracted from measurements on YbRh_2Si_2 [75]. The solid curve is fitted with the function given by Eq. (7).

We next consider the effect of a magnetic field B on the spin-lattice relaxation rate $1/(T_1 T)$. Referring to panel (A) of Fig. 11, which shows the normalized spin-lattice relaxation rate $1/(T_1 T)_N$ at fixed temperature versus magnetic field B , it is seen that increasing B progressively reduces $1/(T_1 T)$, and that as a function of B , there is an inflection point at some $B = B_{\text{inf}}$, marked by the arrow. To clarify the scaling behavior in this case, we normalize $1/(T_1 T)$ by its value at the inflection point, while the magnetic field is normalized by B_{inf} . Taking into account the relation $1/(T_1 T)_N \propto (M^*)^2$, we expect that a strongly correlated Fermi system located near its quantum critical point will exhibit behavior similar to $1/(T_1 T)_N$ [23, 24, 32, 65]. Based on this reasoning, it follows that with application of magnetic fields at fixed temperature, the coefficient W_r behaves like the spin-lattice relaxation rate shown in Fig. 11, i.e., $W_r \propto 1/(T_1 T)$ [24, 32, 65]. Significantly, panel A of Fig. 11 shows that the Herbertsmithite $\text{ZnCu}_3(\text{OH})_6\text{Cl}_2$ [78] and the HF metal $\text{YbCu}_{5-x}\text{Au}_x$ [79] do in fact show the same behavior for the normalized spin-lattice relaxation rate. As indicated in Fig. 11, for $B \leq B_{\text{inf}}$ (or $B_N \leq 1$) the normalized relaxation rate $1/(T_1 T)_N$ depends weakly on the magnetic field, while it diminishes at the higher fields [23, 24, 32, 65]. Panel B of Fig. 11 reports results

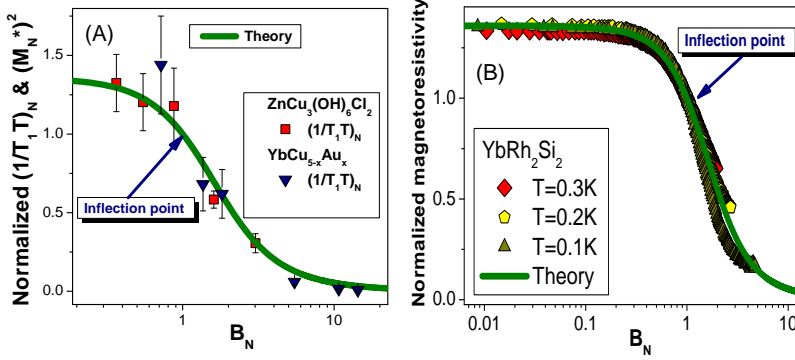


Fig. 11 (Color online) Panel (A). Normalized spin-lattice relaxation rate $(1/T_1T)_N$ at fixed temperature as a function of magnetic field. Data for $(1/T_1T)_N$ extracted from measurements on $\text{ZnCu}_3(\text{OH})_6\text{Cl}_2$ are shown by solid squares [78] and those extracted from measurements on $\text{YbCu}_{5-x}\text{Au}_x$ at $x = 0.4$, by the solid triangles [79]. The inflection point at which the normalization is taken is indicated by the arrow. Panel (B). Magnetic field dependence of the normalized magnetoresistance ρ_N , extracted from LMR of YbRh_2Si_2 at different temperatures [80] listed in the legend. The inflection point is shown by the arrow. In both panels (A) and (B), the calculated result is depicted by the same solid curve, tracing the scaling behavior of $W_r \propto (M^*)^2$ (see Eq. (10)).

for the normalized magnetoresistance

$$\rho_N(y) \equiv \frac{\rho(y) - \rho_0}{\rho_{inf}} = (M_N^*(y))^2 \quad (9)$$

versus normalized magnetic field $y = B/B_{inf}$ at the three temperatures shown in the legend. Here ρ_{inf} and B_{inf} are the longitudinal magnetoresistance (LMR) and magnetic field, respectively, taken at the inflection point indicated by the arrow in panel B of Fig. 11. Both theoretical (solid line) and experimental (symbols) curves have been normalized by their inflection points, which also reveal the scaling behavior: The scaled curves at different temperatures merge into a single curve as a function of the variable B/B_{inf} to establish scaling behavior over three orders in this normalized magnetic field. Taking into account Eq. (8), we obtain

$$W_r \propto 1/(T_1T)_N \simeq \rho_N \simeq (M_N^*)^2 \propto B^{-4/3}. \quad (10)$$

We thus predict that the thermal resistivity of $\text{ZnCu}_3(\text{OH})_6\text{Cl}_2$ behaves like the magnetoresistance of the archetypical HF metal YbRh_2Si_2 , and we conclude that application of a magnetic field B leads to a crossover from NFL to LFL behavior and to a significant reduction in both the relaxation rate and the thermal resistivity. We note that in order to directly observe a possible gap, it will also be crucial to carry out measurements of low-energy inelastic neutron scattering on single crystals of $\text{ZnCu}_3(\text{OH})_6\text{Cl}_2$ subject to a magnetic field that drives the system toward

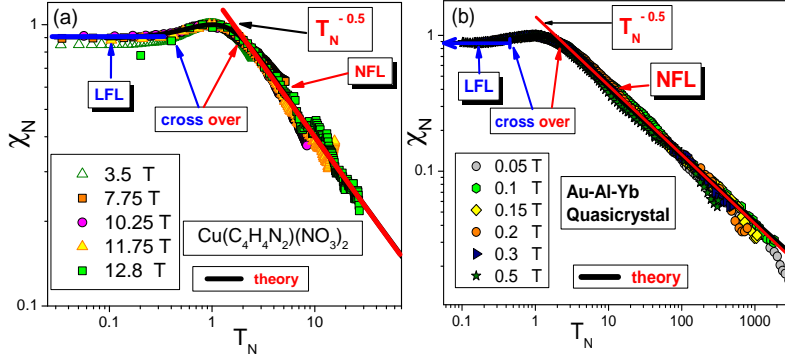


Fig. 12 (Color online) Normalized magnetic susceptibility χ_N extracted from measurements in magnetic fields H (shown in the legend) on CuPzN [81] (panel (a)) and on the $\text{Au}_{51}\text{Al}_{34}\text{Yb}_{15}$ quasicrystal [46] (panel (b)). Our corresponding theoretical curves, merged in the scale of the figure, are drawn as the solid lines tracing the scaling behavior. Panels (a) and (b) demonstrate that the dependence χ_N versus T_N for CuPzN and for the quasicrystal has three distinctive regions: LFL, crossover, and NFL, showing behavior $\chi_N \sim T_N^{-0.5}$ in the latter regime (orange curve).

LFL behavior, since in that case the contribution coming from supposed impurities is negligible, as addressed above for the spin susceptibility χ .

3.4 One-dimensional spin liquids and quasicrystals

To compare the scaling behavior of one-dimensional (1D) SCQSL with that found in other HF compounds such as the quasicrystal $\text{Au}_{51}\text{Al}_{34}\text{Yb}_{15}$, we turn to Fig. 12, which portrays the comparison between the normalized susceptibility χ_N extracted from experiments on the insulator $\text{Cu}(\text{C}_4\text{H}_4\text{N}_2)(\text{NO}_3)_2$ (CuPzN), holding 1D spin liquid, [81] (panel (a)), $\text{Au}_{51}\text{Al}_{34}\text{Yb}_{15}$ [46] (panel (b)), and the theory developed for quasicrystals and 1D SCQSL [33, 35]. For more than three decades in normalized temperature there is very good agreement between the theory and the experimental data. The double-log scale used for the plots reveals the universal dependence $\chi_N \sim T_N^{-0.5}$. Comparison of panels (a) and (b) indicates that in both CuPzN and $\text{Au}_{51}\text{Al}_{34}\text{Yb}_{15}$, the normalized susceptibility χ_N of the 1D SCQSL has three regions of characteristic behavior: the low-temperature LFL part, the medium-temperature crossover region where the maximum occurs, and the high-temperature NFL part with the distinctive temperature dependence $T_N^{-0.5}$. The absolute values of the thermodynamic functions obviously depend on the properties of the individual system in question. The universal features and behavior shared by these systems have only been revealed by means of the normalization procedure based on internal scales [23, 24, 33].

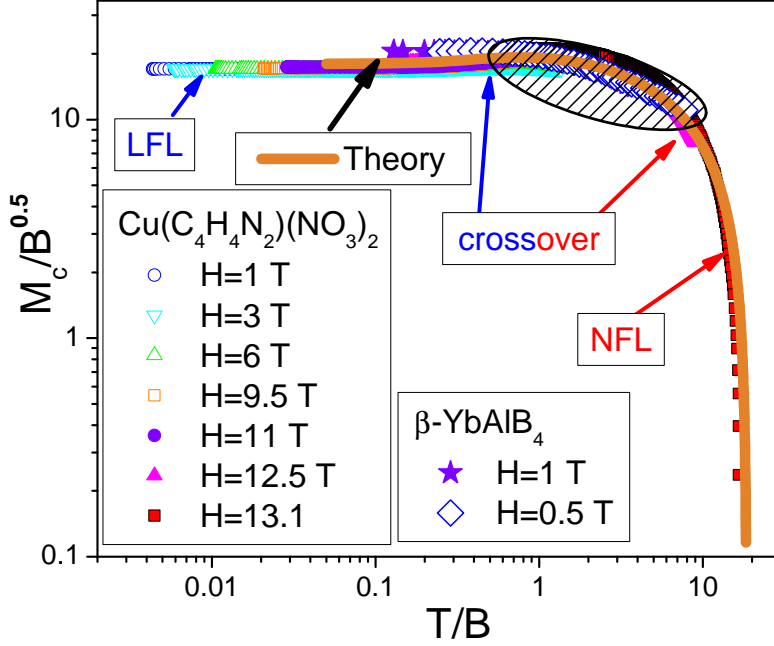


Fig. 13 (Color online) Scaling dependence of the function M_c/\sqrt{B} ($M_c = M_s - M$, $B = H_s - H$) on $(T/B)_N$ for CuPzN. Experimental data are taken from Refs. [27, 81, 82]. The curves correspond to different magnetic fields H listed in the legends. LFL, crossover, and NFL regions are shown. The theoretical dependence is represented by the solid curve [35].

As a final exercise, we trace the scaling behavior of the function $(M_s - M)/\sqrt{B}$ with respect to T/B , applied $B = H_s - H$, where H is the applied magnetic field while M_s and H_s denote respectively the saturation magnetization and saturation magnetic field [27, 35, 81, 82]. The corresponding theoretical dependence can be inferred from Eqs. (3) and (5) exploiting the fact that the magnetization is related to the susceptibility χ via $M = \int \chi dH$, where $\chi \sim M^*(T, H)$ is the magnetic susceptibility. Then, having the effective mass $M^*(T, H)$ from the interpolative solution (3) of the Landau equation, and setting $M_s - M = M_c$, we may obtain the corresponding theoretical dependence [35]

$$\frac{M_c}{\sqrt{B}} = a + \frac{M_s - M}{\sqrt{H_s - H}}, \quad (11)$$

as a function of $T/B = T/(H_s - H)$. That this result is in good agreement with the experimental facts may be seen from Fig. 13 which illustrates the scaling behavior of the magnetization M_c . This behavior, expressed by Eq. (11) and tracked by the solid curve, is indistinguishable from the dependence $M_c/B^{0.5}$ versus T/B

extracted from the experimental data [27, 81, 82], a remarkable coincidence. According to Fig. 13, LFL regime occurs at $T \ll B$, the crossover around $T \sim B$, and the NFL regime $T \gg B$, this being the case for HF compounds that behave like the HF superconductor β - YbAlB₄, the quasicrystal Au₅₁Al₃₄Yb₁₅, the SCQSL of ZnCu₃(OH)₆Cl₂, and the 1D SCQSL of CuPzN [23, 24, 33, 35].

3.5 Summary

To summarize the essence of this section, we have demonstrated that both the impurity model of Herbertsmithite ZnCu₃(OH)₆Cl₂ and the existence of a spin gap in this compound are problematic, as they contradict established properties of this system and are not supported by detailed considerations of its thermodynamics and relaxation properties in magnetic fields. In conclusion, we recommend that measurements of heat transport in magnetic fields be conducted to clarify the nature of the quantum spin-liquid this system. We also have suggested that measurements of low-energy inelastic neutron scattering on ZnCu₃(OH)₆Cl₂ single crystals be performed in magnetic fields. In such a study the contribution coming from supposed impurities would be negligible. We have also shown that the strongly correlated quantum spin liquids existing in ZnCu₃(OH)₆Cl₂ and CuPzN exhibit the same universal behavior as that of other HF compounds, thus providing empirical evidence for a new state of matter related to the presence of flat bands.

4 Precursors of fermion condensation in a gas of 2D ultra cold fermionic atoms

Here we propose a simple model that describes the appearance of precursors (at low but finite temperatures) of fermion condensation (FC) [24] in two-dimensional ensembles of ultracold fermionic atoms, interacting with coherent resonant light. Latter interaction permits to introduce spin-orbit-like and Zeeman - like atom couplings, which at low temperatures drive the system to FCQPT. We note that FC can take place in finite systems as well [23, 24, 48]. We obtain the system phase diagram in the $H - \gamma$ (H is above Zeeman - like field and γ is a strength of interatomic interaction) variables. We show that thermodynamic (magnetic moment and spin susceptibility) and spectroscopic (photon absorption spectra) characteristics of the system exhibit peculiar features due to FC precursor realization. These features can be regarded as FC fingerprints in the system under consideration. Recent progress in achieving highly coherent light-atom interactions in cold atomic matter allows researchers to realize new quantum degrees of freedom such as atomic pseudospin. This pseudospin is related to the coupling of light to the hyperfine structure of the atomic spectrum and can be realized even for bosonic atoms having zero total physical spin like ⁸⁷Rb isotope. Since the atoms coupling to coherent highly resonant light strongly depends on the atom velocity, the atomic motion generates a linear (in the atomic momentum) pseudospin - momentum interaction. This effect produces an artificial analog of the spin-orbit coupling, linear both in the atomic momentum and pseudospin. This interaction formally resembles the famous spin-orbit coupling of electric charge carriers in solids. One can

also produce an artificial magnetic field acting on the atomic pseudospin and corresponding to a strong Zeeman - like interaction. These studies have been comprehensively reviewed in Refs. [83–88] including cold bosons and their Bose-Einstein condensates as well as cold Fermi gases like ^{40}K and ^6Li [89, 90]. Very recently, the above fictitious spin-orbit coupling and Zeeman field in the two-dimensional (2D) Fermi gas of ^{40}K [91] has been reported. It has been shown that cold atom systems can generate spin-orbit coupling and Zeeman-like splitting of the order of the particles kinetic energy. To the best of our knowledge, such high spin-orbit and Zeeman couplings can barely be realized in condensed matter. If they do, this might open a venue to qualitatively new manifestations of above interactions including appearance of new quantum states of condensed matter.

One of the most interesting properties of cold matter is the variety of interparticle interactions manifestations. For Bose-Einstein condensates they are accurately described by the Gross - Pitaevskii equation. For cold fermions, these manifestations may be ferromagnetic fluctuations (the fermionic isotope ^6Li [92]), at relatively strong interatomic interactions. The effect of above fluctuations on the spin drag was considered theoretically in While the actual quantum phase mean field approximation in Ref. [93]. Yet another manifestation of the strong interactions between fermionic atoms may be the realization of condensation - like phenomenon FC, see Ref. [23, 24, 56], generating flat (i.e. wave vector \mathbf{k} independent so that corresponding quasiparticle cannot propagate) portions in the quasiparticles (or real particles) spectrum (energy-momentum relation). These flat portions generate the deviation of the initial (i.e. that without FC) Fermi distribution $n(\mathbf{k})$ from step function ($n(k < k_F) = 1$, $n(k > k_F) = 0$, k_F is Fermi wave vector) at $T = 0$. Namely, in these flat portions of the spectrum (i.e. in FC phase) $0 < n(\mathbf{k}) < 1$, while out of them $n(\mathbf{k})$ is either 1 or 0, see Refs. [24, 56, 94–96] for details. Recently, Yudin et al. [96] proposed to observe FC - like effects (related to the emergence of flat portions of the spectrum) in optical lattice systems of ultracold fermions with a van Hove singularity in the Brillouin zone.

While the actual quantum phase transition to the FC state is envisioned to occur zero temperature, we demonstrate here a two-dimensional atomic Fermi gases with the fictitious spin-orbit coupling and magnetic field described above can exhibit a finite-temperature state that may properly be regarded as a precursor of a actual (or hypothetical) fermion condensation at $T = 0$. We remark that the entropy problem of fermion condensation at $T = 0$ is considered in Section 5, where we show that the entropy of the system in question vanishes at $T \rightarrow 0$ [23]. Our consideration of a finite temperature state is dictated by the experimental situation [83–88], in which very low ($1.5 \cdot 10^{-7}$ K) but nonzero temperatures are realized in the presence of unavoidable photon-atom collisions. We proceed to construct the $H - \gamma$ phase diagram of the system in which the FC precursor can potentially occur (H being the fictitious Zeeman field and γ the strength of the spin-orbit interaction). Also, we calculate the magnetic moment and spin susceptibility as functions of the strength H_z of the artificial magnetic field. The resulting dependences have distinctive features in the range of magnetic fields where FC precursor state can be realized. Such features may be considered experimental fingerprints of FC precursor state. Another proposed fingerprint is of spectroscopic nature and involves the photonic absorption spectrum.

4.1 Theoretical formalism

4.1.1 Ideal 2D fermionic gas

We begin with the Hamiltonian of ideal 2D gas of fermionic particles (we use atomic units where $\hbar = 1$)

$$\mathcal{H}_0 = \frac{k_x^2 + k_y^2}{2m} + \alpha(k_x \sigma_y - k_y \sigma_x) + H_z \sigma_z. \quad (12)$$

Here the first term is kinetic energy, second and third ones are, respectively, the (artificial) spin-orbit and Zeeman interaction terms. Accordingly, α is dimensional (fictitious) spin-orbit interaction constant, H is a (also fictitious) magnetic field (in energy units) and $\sigma_{x,y,z}$ are Pauli matrices.

The eigenvalues of the Hamiltonian (12) have the form ($k^2 = k_x^2 + k_y^2$)

$$E_{\pm} = \frac{k^2}{2m} \pm \sqrt{H_z^2 + \alpha^2 k^2}. \quad (13)$$

The corresponding normalized eigenvectors (spinors) read

$$\begin{aligned} |-\rangle &= \frac{1}{\sqrt{\alpha^2 k^2 + Q_{\mathbf{k}+}^2}} \begin{pmatrix} \alpha k \\ -ie^{i\varphi_{\mathbf{k}}} Q_{\mathbf{k}+} \end{pmatrix}, \\ |+\rangle &= \frac{1}{\sqrt{\alpha^2 k^2 + Q_{\mathbf{k}-}^2}} \begin{pmatrix} \alpha k \\ -ie^{i\varphi_{\mathbf{k}}} Q_{\mathbf{k}-} \end{pmatrix}, \end{aligned} \quad (14)$$

where $Q_{\mathbf{k}\pm} = H_z \pm \sqrt{H_z^2 + \alpha^2 k^2}$, $\varphi_{\mathbf{k}} = \arctan(k_y/k_x)$.

It is instructive to study the spectrum of the noninteracting gas (13) as the classification of states remains the same for a gas with interaction. Namely, the spectrum (13) has two branches, determined by $E_+(k, H_z)$ and $E_-(k, H_z)$, where $E_+ > E_-$ (Fig.14). It is seen from Fig.14 (see also Eq. (13)) that at $H_z = 0$ the spectrum has minimum at $m\alpha$. At nonzero fields $H_z \neq 0$ a gap opens between E_+ and E_- , but at $H_z < m\alpha^2$ the lower branch E_- still has shape with one maximum at $k = 0$ and minimum. At high magnetic fields $H_z > m\alpha^2$ both branches of the spectrum have a parabolic - like shape with one minimum at $k = 0$. Also, the chemical potential μ (see Eq. (20) below) is reported on the panels, showing that the states of only the branch E_- are occupied. This fact remains valid also in the non-ideal, interacting fermionic gas case.

Simple analytical calculation confirms the above behavior. Namely, the condition of extrema of $E_-(k, H_z)$ (13) yields two roots at $H_z \neq 0$

$$k_1 = 0, k_2 = \sqrt{m^2 \alpha^2 - \frac{H_z^2}{\alpha^2}}, \quad (15)$$

where k_1 corresponds to a maximum, and k_2 to a minimum. At $H_z = 0$ the spectrum consists of branches of parabolas $E_{\pm 0} = k^2/(2m) \pm \alpha k$, with E_{-0} having a minimum at

$$k_0 = m\alpha. \quad (16)$$

The root k_2 (15) exists only if the expression under square root is positive, i.e. $m^2\alpha^2 > H_z^2/\alpha^2$ or $H_z < H_0 = m\alpha^2$. We note here that at $H_z = H_0$ the second derivative $d^2E_{k-}/dk^2 = 0$, which means an infinite effective mass in this point. We also calculate the values of $E_{k\pm}$ in the extrema to obtain

$$\begin{aligned} E_{k\pm}(k=0) &= \pm H_z, \\ E_{k-}(k=k_2) &= -\frac{1}{2} \left[m\alpha^2 + \frac{H_z^2}{m\alpha^2} \right], \quad H_z < m\alpha^2, \end{aligned} \quad (17)$$

which is in agreement with numerical calculations from Fig. 14.

To study further the occupation numbers $n_{k\pm}$

$$n_{k\pm} = \left\{ 1 + \exp \left[\frac{E_{k\pm} - \mu}{T} \right] \right\}^{-1}, \quad (18)$$

we need to determine the chemical potential μ , which is the same for both E_+ and E_- branches as our system is in thermodynamic equilibrium. This can be done from the definition of particles (or quasiparticles) density ρ [97]

$$\int (n_{k+} + n_{k-}) \frac{d^2k}{(2\pi)^2} = \rho, \quad \rho = ak_0^2, \quad 0 < a < 4. \quad (19)$$

Here we use the customary definition [83] of cold fermionic atoms density via wave vector k_0 (16). As in the vast majority of experimentally realizable cases, the occupation numbers even for interacting gas (see, e.g. Ref. [83]) depend on k modulus only, the expression (19) can be further simplified after angular integration to give

$$\int_0^\infty (n_{k+} + n_{k-}) k dk = 2\pi a m^2 \alpha^2. \quad (20)$$

The equation (20) will be used now and subsequently (for the interacting case) to determine the functions $\mu_{\pm}(T, H_z)$ at finite temperatures.

The occupation numbers $n_-(k)$, corresponding to the only branch $E_-(k)$ with occupied states, are portrayed in Fig. 15. It is seen, that (fictitious) spin-orbit interaction generates non-typical dependence $n_-(k)$. Really, while normally $n(k)$ has step ($T = 0$) or "blurred step" ($T \neq 0$) behavior, at $H_z < m\alpha^2$ (when the spin-orbit interaction is important, which is most pronounced at $H_z = 0$) we have $n_-(k)$ to be of "II" shape. At high magnetic fields $H_z > m\alpha^2$, the spin-orbit interaction becomes negligible and the ordinary shape of $n_-(k)$ restores. The latter features of $n_-(k)$ shape is also inherent in the interacting case. Below we will also see that FC precursor behavior with flat, dispersionless portions of the spectrum $E_-(k)$ (our analysis shows that for the problem under consideration, the branch $E_+(k)$, even if occupied, never has FC-like behavior) will occur both at $H_z < m\alpha^2$ and $H_z > m\alpha^2$ depending on constant a (responsible for atoms concentration in a gas) in the expression (19).

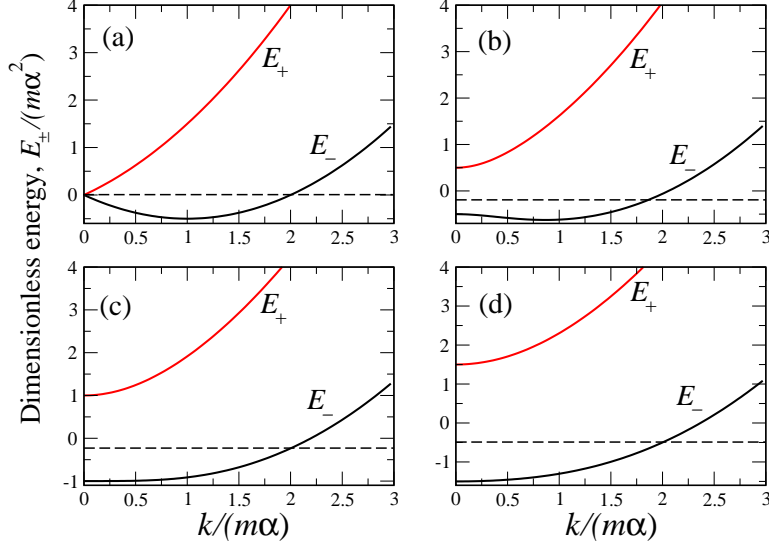


Fig. 14 (Color online) Spectrum of the ideal 2D gas of fermionic atoms consisting of two branches E_- (black curves) and E_+ (red curves). The energies E_{\pm} depend on the artificial magnetic field strength H_z . Panels (a)-(d) correspond to four cases: (a) $H_z = 0$, (b) $H_z = 0.5m\alpha^2$, (c) $H_z = m\alpha^2$ (critical value, when double-well character of $E_-(k)$ disappears), and (d) $H_z = 1.5m\alpha^2$. At $H_z \neq 0$ a gap opens between E_+ and E_- . Horizontal dashed lines correspond to the chemical potential μ at $T = 0.01m\alpha^2$, determined self-consistently from Eq. (20) at the characteristic value $a = 1/\pi$ corresponding to $\mu = 0$ at $H_z = 0$. Occupied states are seen to be present only for the E_- branch.

4.1.2 Interacting fermionic gas

The ground state energy of the interacting, non-ideal gas of cold fermionic atoms can now conveniently be written in the basis (14), diagonalizing the ideal fermionic gas Hamiltonian (12). In the spirit of Ref. [83], it consists of the ideal gas spectrum (13) and all possible matrix elements $g_{\mathbf{k},\mathbf{k}',\alpha,\beta} \equiv \langle \alpha, \mathbf{k}' | \beta, \mathbf{k} \rangle$ ($\alpha, \beta = \pm$), playing a role of interaction term. To be specific, the ground state energy functional reads

$$\begin{aligned}
 W \equiv \langle \mathcal{H} - \mu N \rangle_G = & \sum_{\mathbf{k}} \left[(E_{\mathbf{k}-} - \mu) n_{\mathbf{k}-} + (E_{\mathbf{k}+} - \mu) n_{\mathbf{k}+} \right] + \\
 & + \gamma \sum_{\mathbf{k}, \mathbf{k}'} \left[g_{\mathbf{k}\mathbf{k}'+} n_{\mathbf{k}+} n_{\mathbf{k}'+} + g_{\mathbf{k}\mathbf{k}'-} n_{\mathbf{k}+} n_{\mathbf{k}'-} \right. \\
 & \left. + g_{\mathbf{k}\mathbf{k}'-} n_{\mathbf{k}-} n_{\mathbf{k}'+} + g_{\mathbf{k}\mathbf{k}'+} n_{\mathbf{k}-} n_{\mathbf{k}'-} \right]. \tag{21}
 \end{aligned}$$

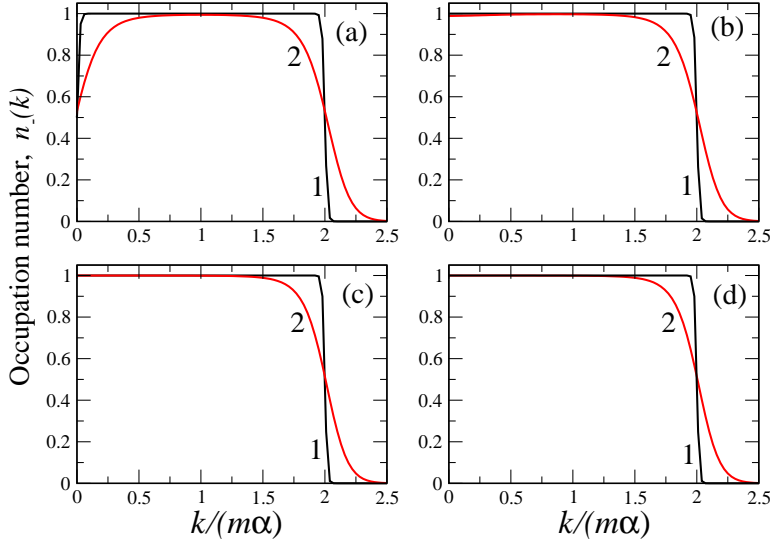


Fig. 15 (Color online) Occupation numbers $n_-(k)$, corresponding to E_- branch (the only having occupied states), of the ideal 2D gas of fermionic atoms for two different temperatures: $T_1 = 0.01m\alpha^2$ (black curves 1) and $T_2 = 0.1m\alpha^2$ (red curves 2). Panels (a) - (d) correspond to H_z values similar to those from Fig. 14. The chemical potentials μ for $T = T_1$ are also the same as those in Fig. 1; $\mu(T_1) \approx \mu(T_2)$.

Here γ is the interaction constant carrying the dimensions of energy and $E_{\mathbf{k},\pm}$ is determined by Eq. (13). Note that while at finite temperatures we should minimize the functional $U = W - TS$, where T is a temperature and S is an entropy (see Ref. [24] and references therein for details), for the experimentally realizable temperatures $T_0 \sim 1.5 \cdot 10^{-7}$ K it is sufficient to minimize the ground state energy only, however, with $n_{\mathbf{k},\pm}$ being temperature dependent by virtue of Eq. (18).

The matrix elements $g_{\mathbf{k},\mathbf{k}',\alpha,\beta}$ may be expressed as

$$g_{\alpha,\beta}(x,x') = \frac{xx'}{S_\alpha(x)S_\beta(x')},$$

$$S_\pm(x) = \sqrt{x^2 + (h \mp \sqrt{h^2 + x^2})^2}. \quad (22)$$

having introduced dimensionless variables $x = k/(m\alpha)$ and $h = H_z/(m\alpha^2)$. We note that the expressions for matrix elements (22) contain an additional term proportional to $\cos \varphi_{\mathbf{k}}$. For isotropic solutions (i.e. dependent only on modulus k), this part gives zero after integration over $\varphi_{\mathbf{k}}$.

Going from summation to integration in Eq. (21) and varying over $n_{\mathbf{k},\pm}$, we arrive at the following set of integral equations for determination of resulting spec-

trum and occupation numbers

$$\begin{aligned}
E_{\mathbf{k}+} - \mu + \frac{\gamma}{(2\pi)^2} \int_0^\infty k' dk' \int_0^{2\pi} d\phi_{\mathbf{k}'} \times \\
\left[g_{\mathbf{k}\mathbf{k}'+} n_{\mathbf{k}'+} + g_{\mathbf{k}\mathbf{k}'-} n_{\mathbf{k}'-} \right] = 0, \\
E_{\mathbf{k}-} - \mu + \frac{\gamma}{(2\pi)^2} \int_0^\infty k' dk' \int_0^{2\pi} d\phi_{\mathbf{k}'} \times \\
\left[g_{\mathbf{k}\mathbf{k}'-} n_{\mathbf{k}'+} + g_{\mathbf{k}\mathbf{k}'+} n_{\mathbf{k}'-} \right] = 0.
\end{aligned} \tag{23}$$

Here the occupation numbers n_{\pm} are related to the spectrum E_{\pm} by the expression (18). The system (23) should be augmented by the equation for self-consistent determination of chemical potential $\mu \equiv \mu(H_z, T)$ (20).

4.2 Results and discussion

To make our (numerical) solution of the set (23) to be physically meaningful, we estimate some characteristic parameters of 2D gas of cold fermionic atoms on the base of experimental situation [83–88]. Typical spin-orbit coupling constant in the above gases is $\alpha = 10$ cm/s. In our calculations we will focus primarily on the fermionic isotope ${}^6\text{Li}$ with mass $m = 10^{-23}$ g. For this atom the characteristic energy related to spin - orbit interaction is $E_c = m\alpha^2 = 10^{-21}$ erg or $6 \cdot 10^{-6}$ meV, which corresponds to temperature $\sim 10^{-5}$ K. The related momentum k_c and concentration ρ_c units are, respectively $k_c = m\alpha = 10^5$ cm $^{-1}$ and $\rho_c = ak_c^2 \approx a \cdot 10^{10}$ cm $^{-2}$, where parameter a is defined in Eq. (19).

The interaction constant γ can be estimated as $\gamma = 4\pi(a_s/w)E_c = 4\pi(a_s/w)M\alpha^2$ [83]. Here a_s is a three-dimensional scattering length, which is of the order of 100 Bohr radii. For two-dimensional case it should be divided by the width of the optically trapped layer ("pancake") w which is typically several microns. With this in mind, the characteristic value of the interaction constant is $\gamma = 4\pi \cdot 0.0053E_c = 7 \cdot 10^{-23}$ erg = $5 \cdot 10^{-7}$ Kelvins. This value is by order of magnitude the same as the characteristic experimentally realizable temperature $T = 1.5 \cdot 10^{-7}$ K due to photon-atom energy transfer. These numerical estimations show that physically meaningful values of the dimensionless temperature are $\tau = T/(M\alpha^2) \sim 0.01 - 0.05$, while other parameters like dimensionless magnetic field h and interaction constant $\gamma_0 = \gamma/(M\alpha^2)$ could be varied to achieve the desired effect.

The set of integral equations (23) has been solved iteratively with respect to Eq. (20) in the above dimensionless variables. The natural choice of zeroth approach in this case is ideal gas spectrum (13). The results are shown in the Fig. 16 in the form of $E_{\pm}(k)$ (a) and $n_{\pm}(k)$ (b) dependences. We choose the parameters H_z and γ , where FC precursor is realized. The temperature (except Fig. 16d, where $T = 0$) has been chosen to be $T = 0.05m\alpha^2$ as this value reflects the experimental situation for ${}^6\text{Li}$ atom. It is seen, that latter phenomenon occurs for the branch $E_-(k)$ only, while $E_+(k)$ remains intact. We did not find contradictions for this regularity: for all possible H_z and γ , the FC (if any) occurs for $E_-(k)$ only. This shows the importance of spin - orbit interaction in the process of FC precursor formation.

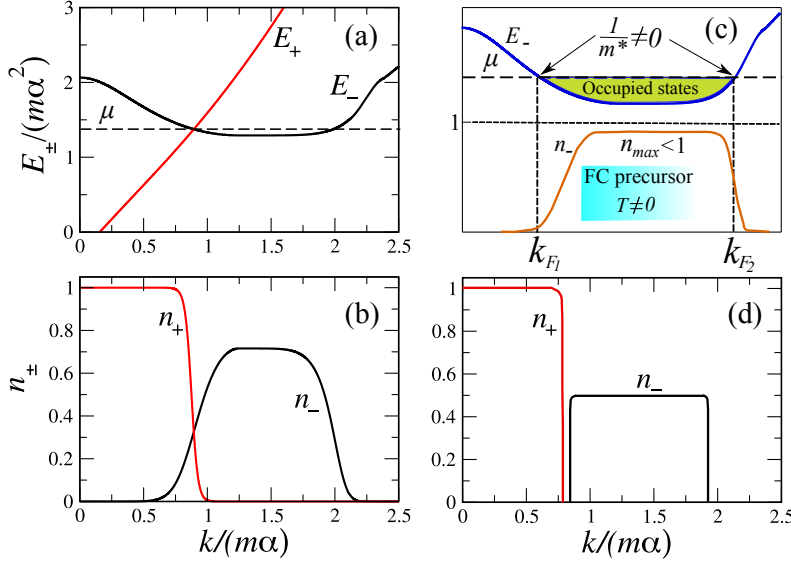


Fig. 16 (Color online) The numerical solution of the set (23) corresponding to the FC precursor realization. The spectrum $E_{\pm}(k)$ is reported in the panel (a) and corresponding occupation numbers $n_{\pm}(k)$ in panel (b). The solution is obtained for $H_z = 0.5m\alpha^2$, $T = 0.05m\alpha^2$ and $\gamma = 12m\alpha^2$. This correspond to the chemical potential $\mu = 1.33785m\alpha^2$ and bottom (flat part) of the $E_-(k)$ $E_{-min} = 1.2917m\alpha^2$. It is seen that FC precursor occurs for $E_-(k)$, while $E_+(k)$ exhibits standard behavior. Panel (c) shows schematically energy spectrum and occupation numbers for the FC precursor state realized at $T \neq 0$. Panel (d) reports the FC precursor state at $T = 0$, see text for details.

The main peculiar feature of our FC precursor phenomenon is the emergence of the flat, dispersionless portion E_{-min} in the bottom of $E_-(k)$ branch with chemical potential μ being very close to it. This implies (Fig. 16b) that corresponding occupation number $n_-(k)$ has its maximal value n_{max} to be less than 1. If we put $T \rightarrow 0$ (which is not the case for all possible H_z and γ where FC precursor occurs), the corresponding dependence $n_-(k)$ will be of exactly "II" shape with $n_{max} = 0.5$, Fig. 16d. Panel (c) of Fig. 16 reports the schematics of energy spectrum and occupation number $n_-(k)$ for our precursor FC state at low but nonzero temperatures. The main feature realized in the FC quantum phase transition at $T = 0$ is exact equality $E(k) = \mu$ at some portion of the spectrum $E(k)$ limited by two wave vectors k_i and k_f (index "i" stands for "initial" and "f" for final), see the book [24] for pedagogical introduction. This, in turn, implies the nonanalytic behavior of $E(k)$ at $k_i < k < k_f$ with all derivatives $d^n E(k)/dk^n = 0$. The zeroth second derivative $d^2 E(k)/dk^2 = 1/m^* = 0$ means the infinite fermion effective mass $m^* \rightarrow \infty$, which is peculiar experimentally observable feature of FC in solids [24, 56]. The occupation number for FC also behaves differently from both stan-

standard Landau Fermi liquid [97] and our FC precursor phase. Namely, its maximal value $n_{max} = 1$ with subsequent gradual decay down to $n = 0$. The decay region is exactly $k_i < k < k_f$ so that initial Fermi wave vector k_f is hidden (or disappears) in FC state. It has been shown by Volovik [98–100], that this is the consequence of the Fermi surface topology altering in the Fermi condensation point at $T=0$. This topology altering can be understood as follows. While the region of the occupied states (between flat part of the spectrum and chemical potential μ) shown in Fig. 16c has finite width, the corresponding region in real FC state [24] is of infinitesimal width. In other words, while our FC precursor can be viewed as "shallow Fermi sea" (between k_{F_1} and k_{F_2} on Fig. 16c), the real FC phase can be regarded as a "beach of Fermi sea". We note that the qualitative FC features are the same for any potential of inter-fermion interaction, yielding real FC phenomenon [24, 56]. Also, the analysis of "FC traces" at finite temperatures [24] shows that the system begins to enter into FC phase at lowering temperatures $T \leq T_f$ when $T \sim E_{min} - \mu$, with T_f being the temperature at which FC starts to define the properties of system in question [23, 24]. As for calculation from Fig. 16a, b $E_{min}/(m\alpha^2) = 1.2917$ and $\mu/(m\alpha^2) = 1.33785$, their difference 0.046 is approximately the temperature $T/(m\alpha^2) = 0.05$. This permits us to hope that our FC precursor has to do with real FC phenomenon at $T = 0$.

The fact that at low temperatures the spectrum $E_{\mathbf{k}-} - \mu \sim T$ can also be shown using following analytical arguments. As both types of occupation numbers $n_{\mathbf{k}\pm}$ obey Fermi-Dirac statistics (18), the corresponding spectra can be represented as

$$E_{\mathbf{k}\pm} - \mu(T) = T \ln \frac{1 - n_{\mathbf{k}\pm}}{n_{\mathbf{k}\pm}}. \quad (24)$$

At low temperatures, say $T < 0.05m\alpha^2$, the occupation numbers $n_{\mathbf{k}\pm}$ can be approximately considered as rectangles, see Fig. 16b, d. This permits to approximately evaluate the integrals in Eqs (23) to constants C_{\pm} , where signs correspond to the equations with $E_{\mathbf{k}\pm}$ respectively. Our numerical calculations show that at $T < 0.05m\alpha^2$ constants C_{\pm} are weakly temperature dependent. Also, as $T \rightarrow 0$ the constant C_- goes to zero while C_+ remains almost the same. This implies that at $T \rightarrow 0$ $E_{\mathbf{k}-} - \mu(T) \approx T \ln((1 - n_{\mathbf{k}-})/n_{\mathbf{k}-}) \sim T$ as for low temperatures $n_{\mathbf{k}-}$ has almost Π shape (Fig. 16b and d) and can be considered as a constant at some interval of k .

At the same time, although in our FC precursor phase the spectrum $E_-(k)$ also has nonanalytic behavior with flat part, this does not imply the infinite effective mass. Really, as it is seen from Fig. 16c, this nonanalytic region does not fall into the intersection between $E_-(k)$ and μ . At these intersection points, labeled k_{F_1} and k_{F_2} , the slope of $E_-(k)$ is finite and hence the effective mass is finite also. We consider this finiteness of the effective mass to be the main difference between our FC precursor and real FC in solids. We call our phenomenon "precursor" as at $T \rightarrow 0$ and eventual $E_{-min} \rightarrow \mu$ many features of real FC will be realized, see Fig. 16d. One of the differences is "I" shape of the occupation numbers $n_-(k)$ (Fig. 16d), which is the consequence of spin-orbit interaction presence. Note that the behavior of occupation numbers both in our FC precursor and in real FC phases does not contradict the Pauli exclusion principle as in both cases $0 < n < 1$.

The next natural question is at which H_z and γ (at a given T) the above FC precursor phenomenon occurs. The phase diagram of the system under consideration

in the dimensionless variables $h = H_z/(m\alpha^2) - \gamma/(m\alpha^2)$ is reported in Fig. 17. The FC precursor phase exists between the branches of parabola-like curves $h(\gamma)$, corresponding to certain concentration parameter a . For instance, at $a = 1/\pi$ (corresponding to $\mu = 0$ for $\gamma = 0$ and $H_z = 0$) and $\gamma = 12$, the FC precursor exists in the field interval $0.16 < h < 0.79$, see Fig. 17. It is seen that for large γ , corresponding to strong interatomic interaction, the FC precursor state starts to exist already at $H_z = 0$. On the other hand, large fields suppress the latter state, which agrees with the behavior of real FC state in solids [24]. Actually, the property that FC precursor exists in our system in some magnetic field interval $H_{min} < H_z < H_{max}$ is in accord with the experimentally observed properties of solids, which can be explained in terms of fermion condensation, see, e.g. Fig.7 of Ref. [35]. Note that at strong interactions the FC precursor state exist also at $H_z > m\alpha^2$, when the dispersion $E_-(k)$ minimum shifts to $k = 0$ and spin-orbit interaction becomes unimportant.

The vertex of parabola-like curves in Fig.17 determines the critical interaction γ_{cr} such that at a given a and $\gamma < \gamma_{cr}$ the FC precursor does not exist. This is because the weak interaction cannot organize the system into collective FC precursor state. The dependence γ_{cr} on concentration parameter a is reported in the inset to Fig.17. The existence of threshold concentration parameter $a_0 = 0.213$ is seen. This shows that for FC precursor realization in the system under consideration the concentration of atoms should be more then threshold value, determined by the parameter a_0 . In other words, to gain such collective state, as FC precursor, we need to have sufficient concentration of strongly enough interacting fermionic atoms. The strong (fictitious) magnetic fields in this case only suppress this collective state similarly to the real magnetic field in solids [24]. Our analysis shows that the dependence $\gamma_{cr}(a)$ approaches a_0 with infinite derivative and that the entire phase diagram depends on temperature. Latter dependence is weak at $T/(m\alpha^2) < 0.05$ so that qualitative features of the phase diagram remain the same at $T \rightarrow 0$.

The frequently experimentally observed quantity in the cold fermionic gases is their spin magnetization

$$\begin{aligned} M = S_z &= \frac{1}{2} \int \left[n_{+,k} \sigma_{z++} + n_{-,k} \sigma_{z--} \right] \frac{d^2k}{(2\pi)^2} = \\ &= \frac{H_z}{2} \int_0^\infty \frac{n_{+,k} - n_{-,k}}{\sqrt{H_z^2 + \alpha^2 k^2}} \frac{kdk}{2\pi}. \end{aligned} \quad (25)$$

Here $\sigma_{z++} \equiv \langle + | \sigma_z | + \rangle$ and $\sigma_{z--} \equiv \langle - | \sigma_z | - \rangle$, where σ_z is Pauli matrix and $| + \rangle$ and $| - \rangle$ are the states (14) of ideal fermionic gas Hamiltonian. The results of calculations of S_z as well as spin susceptibilities $\chi = M/H_z$ and $\chi_{dif} = dM/dH_z$ at $T/(m\alpha^2) = 0.05$ are reported in Fig. 18. It is seen that qualitative behavior of magnetizations and susceptibilities is almost similar for the case of presence ($\gamma = 12$) or absence ($\gamma = 10$) of the FC precursor behavior. The main difference is the "hump" in the magnetization near the upper magnetic field boundary of FC precursor existence at $\gamma = 12$. This "hump" and subsequent faster (then that at $\gamma = 10$) decay of magnetization in this region generates a "well" in the differential susceptibility dM/dh , see upper panel of Fig. 18. The magnetization "hump" and corresponding differential susceptibility "well" near the upper field boundary of FC precursor existence can be well regarded as possible experimental "finger-

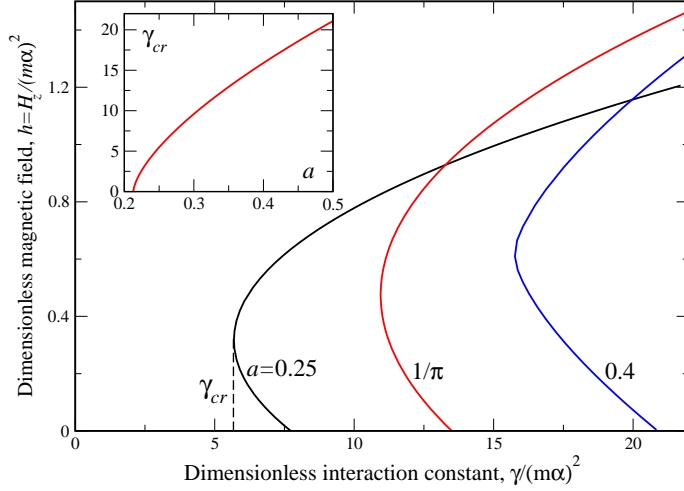


Fig. 17 (Color online) The phase diagram of the system under consideration in the variables $h - \gamma$ at $T = 0.05m\alpha^2$ and different concentration parameters a (Eq. (19), numbers near curves). The FC precursor is realized inside (i.e. between the branches) of parabola-like curves at each a . Inset portrays the dependence of critical interaction constant γ_{cr} (taken at the curves vertices, shown as an example for the curve $a = 0.25$ by dashed line) on parameter a . At $a < 0.213$ the FC precursor does not exist at any h and γ . (Color figure online.)

prints” of this behavior. Although the same maximum and minimum take place also for ”no FC” case $\gamma = 10$, they are much less pronounced than those for $\gamma = 12$ and situated at much smaller fields. Our calculations at $T/(m\alpha^2) = 0.025$ show that both magnetization and susceptibilities are almost the same as those at $T/(m\alpha^2) = 0.05$. This confirms our statement that above peculiar features survive at temperature lowering and thus may be regarded as experimental manifestations of possible FC precursor realization in ultracold fermionic atom gas. To determine the fields range, when possible FC precursor is realized experimentally, the detailed comparison between experimental and theoretical magnetization and susceptibility curves are needed.

The important spectroscopic manifestation of the FC precursor state is the study of the photonic absorption spectra, which intensity I can be related to the occupation numbers n_+ and n_- in a simple manner

$$I(\omega) = \frac{1}{2} [n_+(1 - n_-) + n_-(1 - n_+)], \quad (26)$$

$$\omega \equiv \omega(k) = |E_-(k) - E_+(k)|.$$

The above absorption spectrum defines the transitions (at a given wave vector and hence the frequency (26)) from occupied states in either E_+ or E_- branch of the spectrum to the corresponding free states at a given k . As the frequency of such

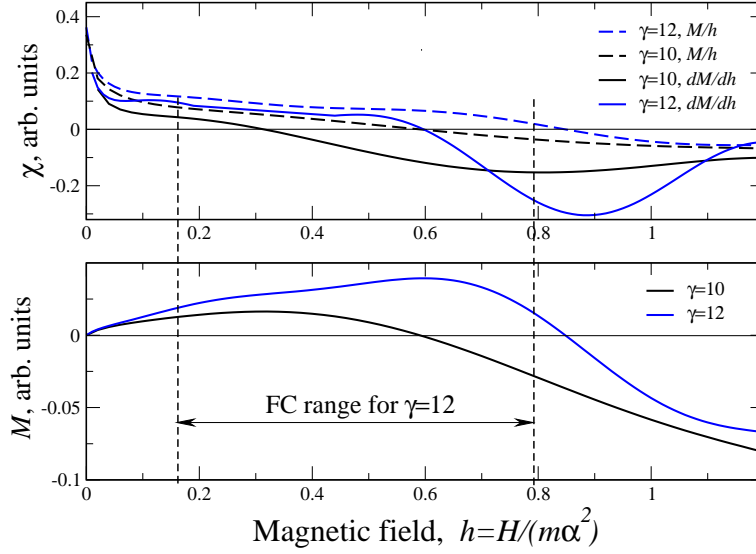


Fig. 18 (Color online) The spin susceptibilities (upper panel) and magnetization (lower panel) of the system under consideration as functions of dimensionless magnetic field h at $T = 0.05m\alpha^2$. Black curves - $\gamma = 10$ (no FC precursor), blue curves - $\gamma = 12$ (the range of magnetic fields, where FC precursor occurs, is shown). Dashed lines correspond to M/H and full lines - dM/dH . (Color figure online.)

transition should always be positive, it is defined as a modulus. To understand better, how these transitions occur, we take a look on Fig. 16a. At small k the states $E_+ < \mu$ are occupied so that transitions go from E_+ to E_- . After the point $E_+ = \mu$, which is almost the same as k_{F_1} in Fig. 16c we have the opposite situation, where the transitions occur from occupied E_- states to free E_+ ones. Such situation is realized until k reaches k_{F_2} (Fig. 16c), whereupon both E_+ and E_- states become free so that the transitions are impossible. This means that point k_{F_2} , where the lower energy branch equals μ is the absorption spectrum termination point.

With this in mind, in Fig. 19 we plot the absorption spectrum for two magnetic field values: $h = 0.12$ (no FC precursor) and $h = 0.5$. The rest of parameters are $a = 1/\pi$, $\gamma = 12$ and $T/(m\alpha^2) = 0.05$. The main difference between FC precursor absence and presence cases is that while in former case the saturation value of absorption line equals one (hence the factor $1/2$ in the definition of $I(\omega)$ (26)), in the latter case this value is always less than one. The origin of such behavior can be seen in Fig. 16b, where n_- for FC precursor phase is plotted. Namely, in this case the saturation value $n_{max} < 1$, see also Fig. 16c. Substitution of this inequality into the expression (14) even for $n_+ = 1$ immediately generates $I_{max} < 1$. This means that most pronounced experimental manifestation of possible FC precursor in ultracold fermionic gases is the fact that saturation amplitude of photonic ab-

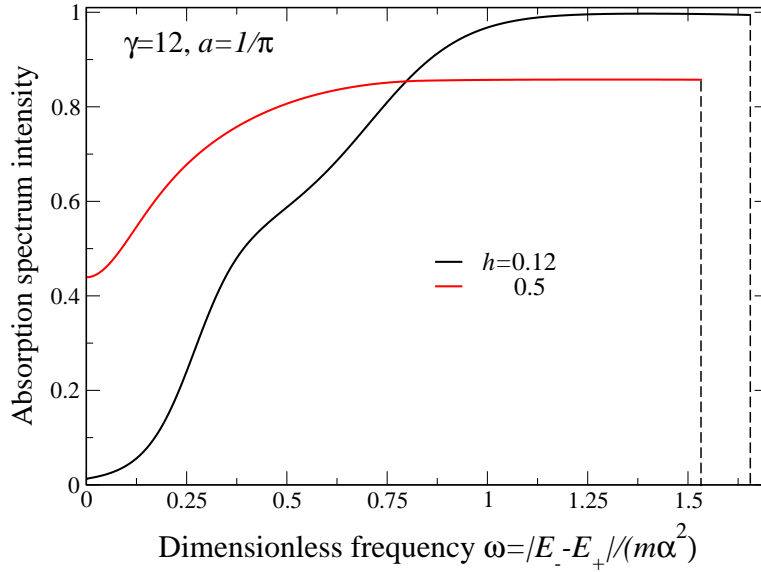


Fig. 19 (Color online) The photonic absorption spectra of the system under consideration at $T = 0.05m\alpha^2$, $a = 1/\pi$ and $\gamma = 12$. Black curves - $h = 0.12$ (no FC precursor), red curves - $h = 0.5$. Vertical dashed lines correspond to spectrum termination points: 1.919 for $h = 0.12$ and 1.678 for $h = 0.5$. (Color figure online.)

sorption spectrum is less than unity. The spectra terminate at respective values of k_{F_2} in dimensionless frequency units: 1.919 for $h = 0.12$ and 1.678 for $h = 0.5$.

4.3 Conclusions

In this second major section, we have devised and explored a simple but realistic model of a 2D gas of cold fermionic atoms, which, at experimentally attainable low temperatures, is found to exhibit features characteristic of a precursor of fermion condensation. We have shown that the presence of a spin-orbit interaction is necessary for the emergence of this new collective state. We have addressed the similarities and differences of and between this state and the real, or fully developed, fermion-condensation phenomenon, which has been studied since the early 1990's [24, 56]. The potential experimental manifestations of possible FC precursor formation have also been considered at some depth. In particular, we predict that in a FC precursor phase the spin magnetization and susceptibility possess specific signatures as functions of the fictitious magnetic field, in the form of a deep minimum of the differential susceptibility. Another predicted manifestation concerns photon absorption spectra, in which case the saturation value near the termination point should become less than unity. To support these predictions,

we have estimated typical system parameters required for realization of the new collective state associated with such FC precursor behavior in ultracold fermionic gases, with the distinct prospect of future experimental confirmation, as the required conditions are expected to be realistically accessible.

5 Overdoped high- T_c superconductors

5.1 Introduction

Strongly correlated Fermi systems hosting a fermion condensate (FC) exhibit unusual properties in both superconducting and (putatively) normal phases. From the fundamental perspective, the presence of a FC breaks both particle-hole symmetry and the time-reversal invariance [101–104]. As a profound consequence, the well-known Leggett theorem [105] is violated. This theorem states that in any superconducting state of an electronic fluid at $T = 0$, the number density of superconducting electrons, n_s , is equal to the total electron number density n_e .

Recent experimental studies of overdoped high- T_c superconductors (HTSC) have revealed strong deviations of their physical properties from those predicted by canonical Bardeen-Cooper-Schrieffer (BCS) theory [106]. Especially confounding, from the conventional vantage, is the documented failure of Leggett's theorem [107]. The observed deviations were found to be surprisingly similar in numerous HTSC samples [106–111]. Measurements of the absolute values of the magnetic penetration depth λ and the phase stiffness $\rho_s = A/\lambda^2$ were carried out on thousands of virtually perfect two-dimensional (2D) samples of $\text{La}_{2-x}\text{Sr}_x\text{CuO}_4$ (LSCO) under variation of doping x and temperature T . (Here $A = d/4k_B e^2$, where d is the film thickness, k_B Boltzmann constant, and e the electron charge.) It was observed that the dependence of the zero-temperature superfluid density (the density of superconductive electrons), written as $n_s = 4\rho_s k_B m^*$ where m^* is the electron effective mass, is proportional to the critical temperature T_c over a wide doping range. This dependence agrees with previous measurements, but is incompatible with the standard BCS description. Most significantly, n_s turns out to be considerably smaller than the BCS density n_{el} of superconductive electrons [106–111], which is approximately equal to the total electron density [112]. These observations, clarifying intrinsic properties of LSCO, have provided unique opportunities for testing and expanding our understanding of the physical mechanisms responsible for high- T_c superconductivity. Our intention here is to show that the physical mechanism responsible for such clear departures from BCS behavior in overdoped LSCO, stems from the topological phase transition giving rise to the FC phenomenon that generates flat bands [23, 24, 56, 98, 100, 113, 114]. We propose that flat bands and an associated extended saddle-point singularity play an important role in the theory of HTSC, as substantiated in Refs. [23, 49, 113–115].

Employing a formalism that accounts for the pertinent fermion-condensation quantum phase transition (FCQPT), we shall now investigate the overdoped LSCO system and show that as soon as the doping x reaches the critical value x_c of this transition, the features of emergent superconductivity begin to differ from those of BCS theory. We will demonstrate that: (i) at $T = 0$, the superfluid density n_s turns out to be only a small fraction of the total density of electrons; (ii) the critical temperature T_c is controlled by n_s rather than by doping, being a linear function

of n_s . Since the FCQPT generates flat electronic bands [24, 56, 98, 100, 113], the system under consideration exhibits non-Fermi liquid (NFL) behavior, notably a resistivity $\rho(T) \propto \alpha T$ varying linearly with temperature. With $x \rightarrow x_c$, the factor α diminishes with decreasing T_c , and the system then exhibits Landau Fermi-liquid (LFL) behavior at $x > x_c$ and low temperatures. These predictions are in good agreement with the recent experimental findings [106, 107, 116].

5.2 Two-component system

Condensed matter theorists have been facing something of a dilemma in attempting to explain the NFL behavior observed in HTSC beyond the critical point where the low-temperature density of states $N(T \rightarrow 0)$ diverges and flat bands can be generated without breaking any ground-state symmetry. (For relevant background and developments, see Refs. [23, 106, 113, 114, 116–118].) In homogeneous matter, such a divergence is associated with the onset of a topological transition at $x = x_c$ signaled by the appearance of an inflection point at momentum $p = p_F$ [23, 28, 114]

$$\begin{aligned} \varepsilon - \mu &\simeq -(p_F - p)^2, \quad p < p_F, \\ \varepsilon - \mu &\simeq (p - p_F)^2, \quad p > p_F, \end{aligned} \quad (27)$$

As a consequence, the FC state and its corresponding flat bands emerge beyond the topological FCQPT [23, 24, 114, 117], while the critical temperature assumes the behavior $T_c \propto \sqrt{x - x_c}$ [115]. These results are consistent with the experimental data [106].

At $T = 0$, the onset of FC in homogeneous matter is attributed to a nontrivial solution $n_0(p)$ of the variational equation [56]

$$\frac{\delta E[n(p)]}{\delta n(p)} - \mu = 0, \quad p \in [p_i, p_f]. \quad (28)$$

Here E is the ground-state energy functional (its variation generating a single-electron spectrum ε), while p_i, p_f denote the limits of the momentum interval within which the solution of Eq. (28) exists (see Refs. [23, 24, 56] for details). To be more specific, Eq. (28) describes the flat band pinned to the Fermi surface, resulting from fermion condensation.

To explain the emergent superconductivity at $x \rightarrow x_c$, we need to examine the consequences of the flattening of the single-particle excitation spectrum $\varepsilon(\mathbf{p})$ (i.e. the appearance of a flat band or bands) in strongly-correlated Fermi systems. (See [23, 24, 113] for recent reviews.) At $T = 0$, the ground state of a system hosting a flat band is degenerate. The occupation numbers $n_0(\mathbf{p})$ of single-particle states belonging to the flat band are continuous functions of momentum \mathbf{p} , in contrast to the standard LFL “step” from 0 to 1 at $p = p_F$, shown by the red dashes (color on-line) in Fig. 20. Thus at $T = 0$ the superconducting order parameter becomes $\kappa(p) = \sqrt{n(p)(1 - n(p))} \neq 0$ in the region occupied by FC [23, 49, 114]. This property is in a stark contrast to standard LFL picture, where at $T = 0$ and $p = p_F$ the order parameter $\kappa(p)$ is necessarily zero, as seen in Fig. 20. Because of the fundamental difference between the FC single-particle spectrum and that of the

remainder of the Fermi liquid, a system having FC is, in fact, a two-component system, separated from the ordinary Fermi liquid by the driving topological phase transition [100, 113, 114]. The range L of momentum space adjacent to μ where the fermion condensate resides is $L \simeq p_f - p_i$, as indicated in Fig. 20.

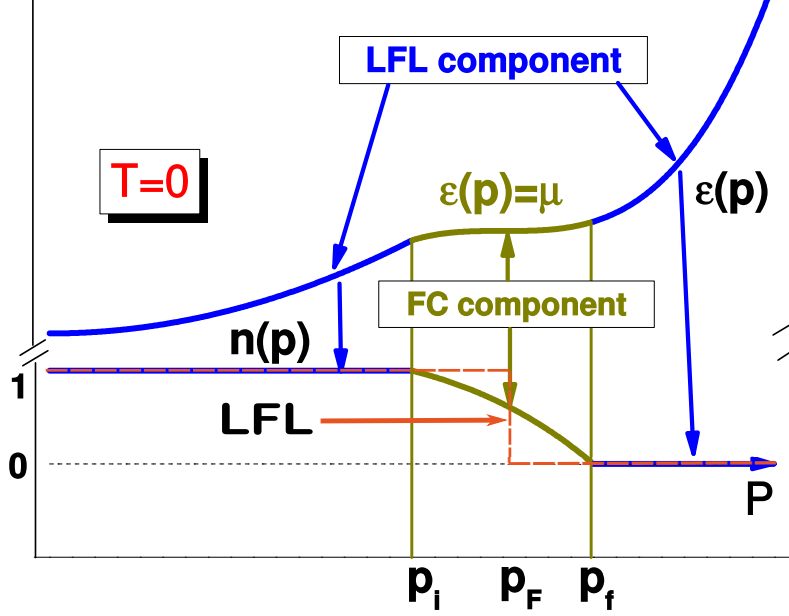


Fig. 20 (Color online) Schematic representation of two-component electron liquid at $T = 0$ with an FC component. Red dashed line (marked “LFL”) shows $n(p)$ for the system *without* a FC, which as ordinary step-function. With the present, the system is separated into two components: (i) a normal Fermi liquid with quasiparticle distribution $n(p < p_i) = 1$ and $n(p > p_f) = 0$. (ii) the FC with $0 < n(p_i < p < p_f) < 1$ and single-particle spectrum $\epsilon(p_i < p < p_f) = \mu$. The Fermi momentum p_F is situated between p_i and p_f .

5.3 Superconductivity in systems with FC

To analyze quantitatively the emergent superconductivity in question, it is convenient to make use of Gor’kov’s formulation for the Green’s functions of a superconductor [23, 97, 119]. For this two-dimensional case, solutions of the Gor’kov equations [23, 97, 119] determine the anomalous and regular Green’s functions $F^+(\mathbf{p}, \omega)$ and $G(\mathbf{p}, \omega)$ of the superconductor:

$$\begin{aligned}
 F^+(\mathbf{p}, \omega) &= \frac{-g_0 \Xi^*}{(\omega - E(\mathbf{p}) + i0)(\omega + E(\mathbf{p}) - i0)}, \\
 G(\mathbf{p}, \omega) &= \frac{u^2(\mathbf{p})}{\omega - E(\mathbf{p}) + i0} + \frac{v^2(\mathbf{p})}{\omega + E(\mathbf{p}) - i0}.
 \end{aligned} \tag{29}$$

Here the single-particle spectrum $\varepsilon(\mathbf{p})$ is determined by Eq. (28) and

$$E(\mathbf{p}) = \sqrt{\xi^2(\mathbf{p}) + \Delta^2(\mathbf{p})}; \quad \frac{\Delta(\mathbf{p})}{E(\mathbf{p})} = 2\kappa(\mathbf{p}), \quad (30)$$

with $\xi(\mathbf{p}) = \varepsilon(\mathbf{p}) - \mu$, where also $\Delta(\mathbf{p})/E(\mathbf{p}) = 2\kappa(\mathbf{p})$. The coefficients $v(\mathbf{p})$ and $u(\mathbf{p})$ of the corresponding Bogoliubov transformation are related to the quasiparticle distribution $n(\mathbf{p})$ and order parameter $\kappa(\mathbf{p})$ by $u^2(\mathbf{p}) = 1 - n(\mathbf{p})$, $v^2(\mathbf{p}) = n(\mathbf{p})$, and $\kappa(\mathbf{p}) = u(\mathbf{p})v(\mathbf{p})$ [97, 119]. The gap Δ and the function Ξ are given by

$$\Delta = g_0 |\Xi|, \quad i\Xi = \int F^+(\mathbf{p}, \omega) \frac{d\omega d\mathbf{p}}{(2\pi)^3}, \quad (31)$$

where g_0 is the superconducting coupling constant. Qualitatively, $F^+(\mathbf{p}, \omega)$ has been interpreted as the wave function of Cooper pairs, and Ξ as the wave function of the motion of these pairs as a whole. Taking Eqs. (30) and (31) into account, we can rewrite Eqs. (29) as

$$\begin{aligned} F^+(\mathbf{p}, \omega) &= -\frac{\kappa(\mathbf{p})}{\omega - E(\mathbf{p}) + i0} + \frac{\kappa(\mathbf{p})}{\omega + E(\mathbf{p}) - i0}, \\ G(\mathbf{p}, \omega) &= \frac{u^2(\mathbf{p})}{\omega - E(\mathbf{p}) + i0} + \frac{v^2(\mathbf{p})}{\omega + E(\mathbf{p}) - i0}. \end{aligned} \quad (32)$$

With $g_0 \rightarrow 0$, one has $\Delta \rightarrow 0$, but Ξ and $\kappa(\mathbf{p})$ remain finite if the spectrum becomes flat, i.e., $E(\mathbf{p}) = 0$. In the interval $p_i \leq p \leq p_f$ Eqs. (32) then become [23, 24, 102]

$$\begin{aligned} F^+(\mathbf{p}, \omega) &= -\kappa(\mathbf{p}) \left[\frac{1}{\omega + i0} - \frac{1}{\omega - i0} \right], \\ G(\mathbf{p}, \omega) &= \frac{u^2(\mathbf{p})}{\omega + i0} + \frac{v^2(\mathbf{p})}{\omega - i0}. \end{aligned} \quad (33)$$

The parameters $v(\mathbf{p})$ and $u(\mathbf{p})$ are determined by the condition that the spectrum should be flat, thus $\varepsilon(\mathbf{p}) = \mu$. It follows from Eqs. (30) and (31) that

$$i\Xi = \int F^+(\mathbf{p}, \omega) \frac{d\omega d\mathbf{p}}{(2\pi)^3} = i \int \kappa(\mathbf{p}) \frac{d\mathbf{p}}{(2\pi)^2} \simeq n_{FC}, \quad (34)$$

where n_{FC} is the density of superconducting electrons forming the FC component (cf. Fig. 20).

We construct the functions $F^+(\mathbf{p}, \omega)$ and $G(\mathbf{p}, \omega)$ in the case where the constant g_0 is finite but small, such that the functions $v(\mathbf{p})$ and $\kappa(\mathbf{p})$ can be found from the FC solutions of Eq. (28). Then Ξ , Δ , and $E(\mathbf{p})$ are given by Eqs. (34), (31), and (30), respectively. Substituting the functions found in this manner into (32), we obtain $F^+(\mathbf{p}, \omega)$ and $G(\mathbf{p}, \omega)$. We note that Eqs. (31) and (34) imply that the gap Δ is a linear function of both g_0 and n_{FC} . Since $T_c \sim \Delta$, we conclude that the critical temperature behaves as $T_c \propto n_{FC} \propto \rho_s$. Since we consider the overdoped HTSC case and FCQPT takes place at $x = x_c$, we also have

$$n_{FC} \propto p_F(p_f - p_i) \propto x_c - x, \quad (35)$$

with $(p_f - p_i)/p_F \ll 1$ [23, 49]. Thus we arrive at the key result

$$n_{FC} = n_s \ll n_{el}. \quad (36)$$

Increasing g_0 causes Δ to become finite, leading to a finite value of the effective mass m_{FC}^* in the FC state [23, 49]:

$$m_{FC}^* \simeq p_F \frac{p_f - p_i}{2\Delta}. \quad (37)$$

An important fact is warrants emphasis at this point. It has been shown in Refs. [23, 24] that within the FC formalism, the BCS relations remain valid if we use the spectrum given by Eq. (37). What this means is that the standard BCS approximation can be used with the a momentum-independent superconducting coupling constant g_0 in the region $|\varepsilon(\mathbf{p}) - \mu| \leq \omega_D$, considering g_0 to be zero outside this region. As usual, ω_D is a characteristic energy proportional to the Debye temperature. With these prescriptions, the superconducting gap depends only on temperature and is determined by the equation [23, 24, 114]

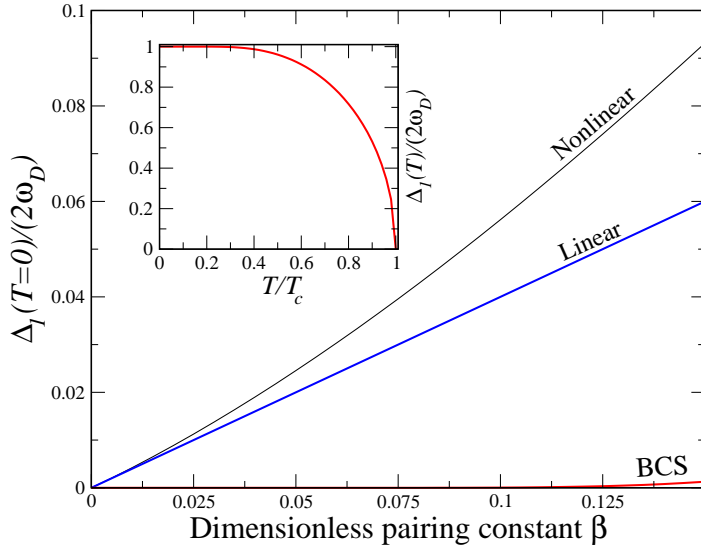


Fig. 21 (Color online) Solution of Eq. (39) in the form $\delta(\beta)$ at $B = 0.4$. The curve labeled “Nonlinear” was obtained by direct numerical solution of the transcendental equation (39). The curve labeled “Linear” plots the linear dependence $\delta = B\beta$, while the curve at the bottom shows the BCS dependence resulting from Eq. (39) at $B = 0$. It is seen that the FC description allows for much higher critical temperatures T_c proportional to superconducting gap $\Delta(T = 0)$ to be reached than the BCS estimate. The inset displays the temperature dependence the superconducting gap in the FC description at $B = 0.4$.

$$\begin{aligned} \frac{1}{g_0} = & N_{FC} \int_0^{E_0/2} \frac{d\xi}{f(\xi, \Delta)} \tanh \frac{f(\xi, \Delta)}{2T} + \\ & + N_L \int_{E_0/2}^{\omega_D} \frac{d\xi}{f(\xi, \Delta)} \tanh \frac{f(\xi, \Delta)}{2T}, \end{aligned} \quad (38)$$

where $f(\xi, \Delta) = \sqrt{\xi^2 + \Delta^2(T)}$ and $E_0 = \varepsilon(p_f) - \varepsilon(p_i) \approx 2\Delta(T=0)$ is a characteristic energy scale. Additionally, $N_{FC} = (p_f - p_F)p_F/(2\pi\Delta(T=0))$ and $N_L = m_L^*/(2\pi)$ are the densities of states of FC and non-FC electrons, respectively, m_L^* being the effective mass of electron of the LFL component, as per Fig. 20. In the limiting case $T = 0$, we have $\tanh(f/(2T)) = 1$ as usual and the remaining integrals can be evaluated exactly. This exercise yields the following equation relating the value $\Delta(T=0)$ with the superconducting coupling constant g_0 :

$$\frac{\delta}{\beta} = B - \delta \ln \delta, \quad (39)$$

where $\beta = g_0 m_L^*/(2\pi)$ is a dimensionless coupling constant, $\delta = \Delta(T=0)/(2\omega_D)$, and $B = (E_F/\omega_D)((p_f - p_F)/p_F) \ln(1 + \sqrt{2})$. The parameter B is seen to depend on the width of FC interval, so at $B = 0$ (i.e., $p_f = p_F$) system is entirely out of the FC and hence in a pure BCS state. In this case the solution of (39) has the standard BCS form $\Delta_{BCS} = \exp(-1/\beta)$. On the other hand, at small β but $B \neq 0$ we obtain a linear relation between the gap and coupling constant, $\delta = B\beta$. This not only differs drastically from the BCS result, it also provides much higher T_c that is directly proportional to $\Delta(T=0)$. Indeed, for the FC solution one typically has [23, 24] $T_c \approx \Delta(T=0)/2$ for the linear regime. Fig. 21 displays results from solution of Eq. (39) in the case of $B = 0.4$ and small β , below 0.15. It is seen that the linear regime of the FC theory already provides much higher T_c values than BCS; indeed, the nonlinear treatment giving the complete numerical solution of Eq. (39) yields even higher T_c . In short, this means that the FC approach is quite capable of explaining the most salient feature of high- T_c superconductivity. Referring again to Fig. 21, the inset shows a plot of the temperature dependence of the FC-derived gap corresponding to Eq. (38), in dimensionless units. This dependence is not specific to the FC approach, as it is qualitatively similar to that of the BCS case. Moreover, variation of the ‘‘FC-parameter’’ B (even setting $B = 0$) does not change the picture qualitatively.

We next analyze the superfluid density n_s for finite g_0 . As seen from Eqs. (34) and (33), n_s emerges when $x \simeq x_c$, and occupies the region $p_i \leq p \leq p_f$. Hence we may write $n_s = n_{FC} \propto x_c - x$, where n_{FC} is the electron density in FC phase. It follows that in the FC phase one has $n_s \ll n_{el} = n_{FC} + n_L$, where n_{el} and n_L are respectively the total density of electrons and the electron density outside the FC phase. We should note that the result $n_s \sim n_{el}$ does is not restricted to BCS theory of superconductivity, but rather is a much deeper property belonging to almost any superfluid system, by virtue of the Leggett theorem [105]. The practical implication of this theorem is that at $T = 0$ in any system exhibiting superfluidity (or superconductivity in the case of charged particles), the number n_s density of particles exhibiting superfluid behavior should not depart substantially from the number density of all liquid particles of the system. In the present case of an electronic fluid, this means that $n_s \approx n_e$, where n_e is the total electron density. However, a condition for this theorem to hold is that the system be T -invariant, i.e.,

possess time-reversal symmetry. Topologically, the FC state is quite non-trivial topologically [24, 98, 103, 104, 113], and lacks this symmetry (also violating CP invariance, i.e., symmetry under combined charge conjugation and parity reversal [23, 104]). The exactly solvable model and general consideration show that the inequality $n_s \ll n_{el}$ is inherent to FC, as it is seen from Eqs. (34) and (36) [23, 24, 49]. Absent some even more exotic mechanism, and in the presence of a host of other favorable experimental observations, it is reasonable to propose that the main contribution to the superconductivity in overdoped high- T_c materials as revealed by the recent experiments [106, 107] has its origin in the FC state. Pairing with such unusual properties can be viewed as a shadow of fermion condensation – a situation foretold by an exactly solvable model long before the experimental observations were obtained by Božović et al. [106] and demonstrating that both the gap and the order parameter exist only in the region occupied by fermion condensate [49]. Thus, the experimental observations [106] can be viewed as a direct experimental manifestation of FC, while another direct experimental manifestation of FC has been done recently [47], where FC phenomenon has been detected in two-dimensional SiGe/Si/SiGe heterostructures.

The essential message of the above deliberations is that fermion condensation entails emergence of a two-component (two-fluid) system that explains, in a natural way, the deficit $n_s \ll n_e$ (inconsistent with BCS) that is observed in overdoped high- T_c materials, while allowing for the observed high critical temperatures.

5.4 Penetration depth, thermodynamic and transport properties

We now address the question: does our FC-based superconductor belongs to the London type. To this end, we recall London's electrodynamics equations, namely

$$\nabla \times \mathbf{j}_s = -(n_s e^2 / m^*) \mathbf{B} \equiv -(n_{FC} e^2 / m_{FC}^*) \mathbf{B}, \quad \nabla \times \mathbf{B} = 4\pi \mathbf{j}_s, \quad (40)$$

where \mathbf{j}_s is a superconducting current. These equations imply a penetration depth

$$\lambda^2 = \frac{m_{FC}^*}{4\pi e^2 n_{FC}}. \quad (41)$$

Comparing this penetration depth with the coherence length $\xi_0 \sim p_F / (m_{FC}^* \Delta)$, we conclude that $\lambda \gg \xi_0$ since the FC quasiparticle effective mass is huge [24]. Thus, the superconductors being considered are indeed of the London type.

It turns out that in the FC phase, the penetration depth is a function not only of temperature, but also of doping degree x . It then follows from Ginzburg-Landau theory that the density of superconducting electrons n_s grows with $T_c - T$, $n_s \sim T_c - T$. On the other hand, as has been discussed in Ref. [106], pressure enhances n_s , meaning that the density x of charge carriers is important. Further, it has been shown [23, 24] that $T_c(x=0) \simeq 2\Delta(T=0)$ in a superconducting phase involving a FC. This allows us to use the relation (41) to plot the penetration depth as a function of temperature and doping in the form

$$\frac{\lambda}{\lambda_0} = \frac{1}{\sqrt{1-y-\tau}}, \quad (42)$$

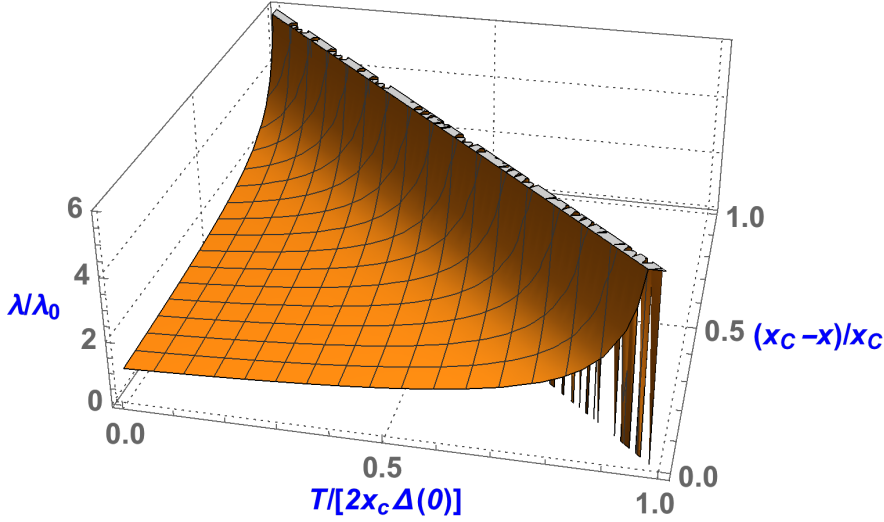


Fig. 22 (Color online) Dependence of the dimensionless penetration depth λ/λ_0 of Eq. (42) on temperature and doping.

where $y = (x_c - x)/x_c$ and $\tau = T/(2\Delta(T=0)x_c)$, with λ_0 combining all proportionality coefficients entering the problem. The dependence (42) is depicted in Fig. 22. Very good qualitative agreement with experimental data (Fig. 2a from Ref. [106]) is seen. In particular, the doping-dependent penetration depth λ becomes infinite at the superconducting phase transition temperature. At zero temperature the divergence of λ occurs at $x \simeq x_c$, corresponding to FC-phase emergence, i.e. at $T = 0$ both superconductivity and the FC phase make their appearance. At higher temperatures, λ becomes divergent in the region $x < x_c$, i.e. deeply inside the FC phase. This produces “traces” of the FC at finite temperatures. In effect, the present approach, based on the hypothesis of a topological FC quantum phase transition, describes the most essential and puzzling features of overdoped HTSC.

The essential features of our dual-component many-fermion model that equip it for success in explaining the unexpected behavior of overdoped high- T_c superconductors stem derived from two distinctive properties of its fermion-condensate component. First, this FC component necessarily involves only a small fraction of the traditional Fermi sphere, thus endowing superfluidity on a number density $n_s \simeq n_{FC}$ of electrons much smaller than the total electron number density n_e . And second, FC superconductivity entails a relation between coupling strength and energy gap (hence T_c), namely Eq. (39), which is altered drastically from that of BCS theory, providing for the much higher critical temperatures observed and predicted.

Another favorable attribute of the two-fluid FC model is consistency with Uemura's law [108]. Since $T_c \propto n_s/m^* \equiv n_{FC}/m_{FC}^*$, we may call upon Eqs. (37) and (41) to derive

$$\frac{\rho_s}{A} = \lambda^{-2} \simeq \frac{n_s}{m^*} \simeq \frac{n_{FC}}{m_{FC}^*} \simeq 2\Delta \simeq T_c. \quad (43)$$

Taking into account $n_{FC} \propto x_c - x$, we find that Eq. (43) reproduces the main results of our analysis, in good agreement with the experimental data [106, 107]. The dependence of T_c on ρ_s is seen to be linear, thus representing the observed scaling law, while T_c is primarily controlled by n_s [106]. We note that the results for underdoped HTSC [108, 109] are similar to those for overdoped HTSC, which suggests an underdoped/overdoped symmetry [106]. Consequently, we find good agreement with Uemura's law in overdoped LSCO as well [106].

It is worth pointing out that for doping levels $x > x_c$ at which FCQPT has not yet occurred, the system is in the LFL phase where the resistivity behaves as $\rho \propto T^2$, indicative of "more metallic" character than that exhibited in the FC phase [101, 106, 116, 117, 120]. Superconductivity as observed appears in the latter phase because the FC phenomenon strongly facilitates the superconducting state. In the "normal" phase at $T > T_c$, FC gives rise to linear T -dependence of the resistivity, $\rho(T) \propto T$ [48, 49, 117, 120], in good qualitative agreement with the experimental data on LSCO and $\text{La}_{2-x}\text{Ce}_x\text{CuO}_4$ [106, 116]. We note that in the transition region $x \simeq x_c$, the behavior $\rho(T) \propto T^\alpha$ is observed with $\alpha \sim 1.0 - 2.0$ [116, 117, 120].

6 Conclusions

Combining analytical considerations with arguments based entirely on experimental grounds, we have shown that data collected on very different strongly correlated many-fermion systems demonstrates a remarkable commonality among them, as expressed in universal scaling behavior of their thermodynamic, transport, and relaxation properties, independently of the great diversity in their individual microstructure and microdynamics. The systems considered range from heavy-fermion metals, to quantum liquids including ^3He films, to insulating compounds possessing one-, two-, and three-dimensional quantum spin-liquid states, to quasicrystals and beyond. The universal behavior exhibited by this class of systems, generically known as heavy-fermion (HF) systems or compounds, being analogous to that commonality expressed in gaseous, liquid, and solid states of matter, leads us to consider such HF systems as manifestations of a new state of matter arising from the presence of flat bands in their excitation spectra. Such flat bands arise from the formation of a fermion condensate (FC) due to a specific quantum phase transition, as it is foretold in 1990 [56].

In order to facilitate experimental observation of the FC state in trapped, ultracold atomic gases, we have formulated and solved a simple yet realistic model that predicts the appearance of fermion-condensation precursors in a two-dimensional ensemble of ultracold fermionic atoms interacting with coherent resonant light. We have shown that thermodynamic characteristics of the system exhibit experimentally observable signatures of FC-precursor realization. Such features can

be regarded as fermion-condensation fingerprints in the system under consideration. We note that the direct experimental manifestation of fermion condensation has been done recently [47], where FC phenomenon has been detected in two-dimensional SiGe/Si/SiGe heterostructures.

We have concluded our study of exemplifications of the new state of matter reached by fermion condensation with an exploration of high- T_c superconductors as potential hosts of fermion condensates. In fact, we have shown that the underlying physical mechanism responsible for the unusual properties of the overdoped compound $\text{La}_{2-x}\text{Sr}_x\text{CuO}_4$ (LSCO) observed recently [106, 107] may very well involve a topological quantum phase transition that induces fermion condensation. Since the topological FC state violates time-reversal symmetry, the Leggett theorem no longer applies. Instead, we have demonstrated explicitly that the superfluid number density n_s turns out to be small compared to the total number density of electrons. We have also shown that the critical temperature T_c is a linear function of n_s , while $n_s(T) \propto T_c - T$. Pairing with such unusual properties is as a shadow of fermion condensation – a situation foretold by an exactly solvable model [49] long before the experimental observations were obtained by Božović et al. [106] and demonstrating that both the gap and the order parameter exist only in the region occupied by fermion condensate. Thus, the experimental observations [106] can be viewed as a direct experimental manifestation of FC. Additionally, we have demonstrated that at $T > T_c$ the resistivity $\rho(T)$ varies linearly with temperature, while for $x > x_c$ it exhibits metallic behavior, $\rho(T) \propto T^2$. Thus, pursuit of a superconductivity formalism adapted to the presence of a fermion condensate captures all the essential physics of overdoped LSCO and successfully explains its most puzzling experimental features, thereby allowing us to close the colossal gap existing between the experiments and Bardeen-Cooper-Schrieffer-like theories. Indeed, these findings are applicable not only to LSCO but also for any overdoped high-temperature superconductor.

Acknowledgements We are grateful to V.A. Khodel for valuable discussions. This work was partly supported by U.S. DOE, Division of Chemical Sciences, Office of Basic Energy Sciences, Office of Energy Research. JWC is indebted to the University of Madeira and its Centro de Ciências Matemáticas for gracious hospitality during his sabbatical residency.

References

1. G.R. Stewart, Rev. Mod. Phys. **73**, 797-855 (2001)
2. H. v. Löhneysen, A. Rosch, M. Vojta, P. Wölfle, Rev. Mod. Phys. **79**, 1015-1076 (2007)
3. C.M. Varma, Z. Nussinov, W. van Saarloos, Phys. Rep. **361**, 267 (2002)
4. M. Vojta, Rep. Prog. Phys. **66**, 2069-2110 (2003)
5. V.I. Belyavsky, Yu.K. Kopaev, Phys. Usp. **49**, 441 (2006)
6. V.R. Shaginyan, M.Ya. Amusia, K.G. Popov, Phys. Usp. **50** 563 (2007)
7. J. Custers, P. Gegenwart, H. Wilhelm, K. Neumaier, Y. Tokiwa, O. Trovarelli, C. Geibel, F. Steglich, C. Pépin, P. Coleman, Nature **424**, 524-527 (2003)
8. T. Senthil, M.P.A. Fisher, Phys. Rev. B **62**, 7850 (2000)
9. T. Senthil, M. Vojta, S. Sachdev, Phys. Rev. B **69**, 035111 (2004)
10. T. Senthil, S. Sachdev, M. Vojta, Physica B **359-361**, 9 (2005)

11. T. Senthil, A. Vishwanath, L. Balents, S. Sachdev, M.P.A. Fisher, *Science* **303**, 1490 (2004)
12. P. Coleman, Lectures on the Physics of Highly Correlated Electron Systems VI, in: F. Mancini (Ed.), American Institute of Physics, New York, 2002, pp. 79-160.
13. P. Coleman, A.J. Schofield, *Nature* **433**, 226 (2005)
14. R. K uchler, N. Oeschler, P. Gegenwart, T. Cichorek, K. Neumaier, O. Tegus, C. Geibel, J. A. Mydosh, F. Steglich, L. Zhu, Q. Si, *Phys. Rev. Lett.* **91**, 066405 (2003)
15. P. Gegenwart, J. Custers, C. Geibel, K. Neumaier, T. Tayama, K. Tenya, O. Trovarelli, F. Steglich, *Phys. Rev. Lett.* **89**, 056402 (2002)
16. N.E. Hussey, *Nature Phys.* **3**, 445 (2007)
17. P. Gegenwart, T. Westerkamp, C. Krellner, Y. Tokiwa, S. Paschen, C. Geibel, F. Steglich, E. Abrahams, Q. Si, *Science* **315**, 969 (2007)
18. P. Coleman, C. P epin, Q. Si, R. Ramazashvili, *J. Phys. Condens. Matter* **13**, R723 (2001)
19. L.D. Landau *Zh. Eksp. Sov. Phys. JETP* **3**, 920 (1956)
20. E.M. Lifshitz, L.P. Pitaevskii, *Statisticheskaya Fizika (Statistical Physics)*, Pt. 2, Nauka, Moscow, 1978; Translated into English, Pergamon Press, Oxford, 1980
21. D. Pines, P. Nozi eres, *Theory of Quantum Liquids*, Benjamin, New York, 1966
22. V.R. Shaginyan, J.G. Han, J. Lee, *Phys. Lett. A* **329**, 108 (2004)
23. V. R. Shaginyan, M. Ya. Amusia, A. Z. Msezane, K. G. Popov, *Phys. Rep.* **492**, 31 (2010)
24. M. Ya. Amusia, K. G. Popov, V. R. Shaginyan, V. A. Stephanovich, *Theory of Heavy-Fermion Compounds*, Springer Series in Solid-State Sciences, **182**, Springer, Heidelberg, New York, Dordrecht, London, 360 p. (2015)
25. V.A. Khodel, J.W. Clark, M.V. Zverev, *Phys. Rev. B* **78**, 075120 (2008)
26. V.A. Khodel, *JETP Lett.* **86**, 721-726 (2007)
27. T. Tomita, K. Kuga, Y. Uwatoko, P. Coleman, S. Nakatsuji, *Science* **349**, 506 (2015)
28. V.R. Shaginyan, A.Z. Msezane, K.G. Popov, J.W. Clark, V.A. Khodel, M.V. Zverev, *Phys. Rev. B* **93**, 205126 (2016)
29. V.R. Shaginyan, A.Z. Msezane, K.G. Popov, V.A. Stephanovich, *Phys. Rev. Lett.* **100**, 096406 (2008)
30. V.R. Shaginyan, A.Z. Msezane, K.G. Popov, *Phys. Rev. B* **84**, 060401(R) (2011)
31. V.R. Shaginyan, A.Z. Msezane, K.G. Popov, V.A. Khodel, *Phys. Lett. A* **376**, 2622 (2012)
32. V.R. Shaginyan, A.Z. Msezane, K.G. Popov, G.S. Japaridze, V.A. Stephanovich, *Europhys. Lett.* **97**, 56001 (2012)
33. V.R. Shaginyan, A.Z. Msezane, K.G. Popov, G.S. Japaridze, V.A. Khodel, *Phys. Rev. B* **87**, 245122 (2013)
34. V.R. Shaginyan, V.A. Stephanovich, K.G. Popov, E.V. Kirichenko, *JETP Lett.* **103**, 32 (2016)
35. V.R. Shaginyan, V.A. Stephanovich, K.G. Popov, E.V. Kirichenko, S.A. Artamonov, *Ann. Phys. (Berlin)*, **528**, 483 (2016)

36. C. Proust, E. Boaknin, R. W. Hill, L. Taillefer, A.P. Mackenzie, *Phys. Rev. Lett.* **89**, 147003 (2002)
37. K. Kadowaki, S.B. Woods, *Solid State Commun.* **58**, 507 (1986)
38. A.J. Millis, A.J. Schofield, G.G. Lonzarich, S.A. Grigera, *Phys. Rev. Lett.* **88**, 217204 (2002)
39. R. Bel, K. Behnia, Y. Nakajima, K. Izawa, Y. Matsuda, H. Shishido, R. Settai, Y. Onuki, *Phys. Rev. Lett.* **92**, 217002 (2004)
40. J. Paglione, M.A. Tanatar, D.G. Hawthorn, E. Boaknin, R.W. Hill, F. Ronning, M. Sutherland, L. Taillefer, C. Petrovic, P.C. Canfield, *Phys. Rev. Lett.* **91**, 246405 (2003)
41. J. Paglione, M.A. Tanatar, D.G. Hawthorn, F. Ronning, R.W. Hill, M. Sutherland, L. Taillefer, C. Petrovic, *Phys. Rev. Lett.* **97**, 106606 (2006)
42. F. Ronning, R.W. Hill, M. Sutherland, D.G. Hawthorn, M.A. Tanatar, J. Paglione, L. Taillefer, M.J. Graf, R. S. Perry, Y. Maeno, A.P. Mackenzie, *Phys. Rev. Lett.* **97**, 067005 (2006)
43. F. Ronning, C. Capan, E.D. Bauer, J.D. Thompson, J.L. Sarrao, R. Movshovich, *Phys. Rev. B* **73**, 064519 (2006)
44. J.D. Koralek, J.F. Douglas, N.C. Plumb, Z. Sun, A.V. Fedorov, M.M. Murnane, H.C. Kapteyn, S.T. Cundiff, Y. Aiura, K. Oka, H. Eisaki, D.S. Dessau, *Phys. Rev. Lett.* **96**, 017005 (2006)
45. S. Fujimori, A. Fujimori, K. Shimada, T. Narimura, K. Kobayashi, H. Namatame, M. Taniguchi, H. Harima, H. Shishido, S. Ikeda, D. Aoki, Y. Tokiwa, Y. Haga, Y. Onuki, *Phys. Rev. B* **73**, 224517 (2006)
46. K. Deguchi, S. Matsukawa, N. K. Sato, T. Hattori, K. Ishida, H. Takakura, T. Ishimasa, *Nature Materials* **11**, 1013 (2012)
47. M. Yu. Melnikov, A. A. Shashkin, V. T. Dolgoplov, S.-H. Huang, C. W. Liu, S. V. Kravchenko *arXiv:1604.08527*
48. V.A. Khodel, V.R. Shaginyan, P. Schuck, *JETP Lett.* **63**, 752 (1996)
49. J. Dukelsky, V. Khodel, P. Schuck, V. Shaginyan, *Z. Phys.* **102**, 245 (1997)
50. N. Oeschler, S. Hartmann, A.P. Pikul, C. Krellner, C. Geibel, F. Steglich, *Physica B* **403**, 1254 (2008)
51. P. Gegenwart, T. Westerkamp, C. Krellner, M. Brando, Y. Tokiwa, C. Geibel, F. Steglich, *Physica B* **403**, 1254 (2008)
52. V.R. Shaginyan, M.Ya. Amusia, K.G. Popov, *Phys. Lett. A* **373**, 2281 (2009)
53. V.R. Shaginyan, M.Ya. Amusia, K.G. Popov, S.A. Artamonov, *JETP Lett.* **90**, 47 (2009)
54. D. Takahashi, S. Abe, H. Mizuno, D. Tayurskii, K. Matsumoto, H. Suzuki, Y. Onuki, *Phys. Rev. B* **67**, 180407(R) (2003)
55. A.W. Rost, S.A. Grigera, J.A.N. Bruin, R.S. Perry, D. Tian, S. Raghu, S.A. Kivelson, A.P. Mackenzie, *Proc. Natl. Acad. Sci. USA* **108**, 16549 (2011)
56. V. A. Khodel, V.R. Shaginyan, *JETP Lett.* **51**, 553 (1990)
57. T.H. Han, J.S. Helton, S. Chu, A. Prodi, D.K. Singh, C. Mazzoli, P. Müller, D.G. Nocera, Y.S. Lee, *Phys. Rev. B* **83**, 100402(R) (2011)
58. J.S. Helton, K. Matan, M.P. Shores, E.A. Nytko, B.M. Bartlett, Y. Qiu, D.G. Nocera, Y.S. Lee, *Phys. Rev. Lett.* **104**, 147201 (2010)
59. J.S. Helton, K. Matan, M.P. Shores, E.A. Nytko, B.M. Bartlett, Y. Yoshida, Y. Takano, A. Suslov, Y. Qiu, J.-H. Chung, D.G. Nocera, Y.S. Lee, *Phys. Rev. Lett.* **98**, 107204 (2007)

-
60. M. A. deVries, K.V. Kamenev, W.A. Kockelmann, J. Sanchez-Benitez, A. Harrison *Phys. Rev. Lett.* **100**, 157205 (2008)
 61. H.J. Liao, Z.Y. Xie, J. Chen, Z.Y. Liu, H.D. Xie, R.Z. Huang, B. Normand, T. Xiang, *Phys. Rev. Lett.* **118**, 137202 (2017)
 62. T.H. Han, M.R. Norman, J.-J. Wen, J.A. Rodriguez-Rivera, J.S. Helton, C. Broholm, Y.S. Lee, *Phys. Rev. B* **94**, 060409(R) (2016)
 63. T. Imai, M. Fu, T.H. Han, Y.S. Lee, *Phys. Rev. B* **84**, 020411(R) (2011)
 64. M. Fu, T. Imai, T.H. Han, Y.S. Lee, *Science* **350**, 655 (2015)
 65. V.R. Shaginyan, A.Z. Msezane, K.G. Popov, G.S. Japaridze, V.A. Khodel, *Europhys. Lett.* **103**, 67006 (2013)
 66. V.R. Shaginyan, M.Ya. Amusia, A.Z. Msezane, K.G. Popov, V.A. Stephanovich, *Phys. Lett. A* **379**, 2092 (2015)
 67. V.R. Shaginyan, M.Ya. Amusia, J.W. Clark, G.S. Japaridze, A.Z. Msezane, K.G. Popov, V.A. Stephanovich, M. V. Zverev, V.A. Khodel, arXiv:1409.4034.
 68. T.H. Han, S. Chu, Y.S. Lee, *Phys. Rev. Lett.* **108**, 157202 (2012)
 69. T.H. Han, R. Chisnell, C.J. Bonnoit, D.E. Freedman, V.S. Zapf, N. Harrison, D.G. Nocera, Y. Takano, Y. S. Lee, arXiv:1402.2693 (2014)
 70. M. Gomilsek, M. Klanjsek, M. Pregelj, H. Luetkens, Y. Li, Q. M. Zhang, A. Zorko, *Phys. Rev. B* **94**, 024438 (2016)
 71. T.H. Han, J.S. Helton, S. Chu, D.G. Nocera, J.A. Rodriguez-Rivera, C. Broholm, Y.S. Lee, *Nature* **492**, 406 (2012)
 72. W. Knafo, S. Raymond, J. Flouquet, B. Fåk, M.A. Adams, P. Haen, F. Lapiere, S. Yates, P. Lejay, *Phys. Rev. B* **70**, 174401 (2004)
 73. B. Fåk, F.C. Coomer, A. Harrison, D. Visser, M.E. Zhitomirsky, *Europhys. Lett.* **81**, 17006 (2008)
 74. V.R. Shaginyan, K.G. Popov, V.A. Khodel, *JETP* **116**, 848 (2013)
 75. C. Stock, C. Broholm, F. Demmel, J. Van Duijn, J. W. Taylor, H.J. Kang, R. Hu, C. Petrovic, *Phys. Rev. Lett.* **109**, 127201 (2012)
 76. M. Yamashita, N. Nakata, Y. Senshu, M. Nagata, H.M. Yamamoto, R. Kato, T. Shibauchi, Y. Matsuda, *Science* **328**, 1246 (2010)
 77. M. Yamashita, T. Shibauchi, Y. Matsuda, *Chem. Phys.* **13**, 74 (2012)
 78. T. Imai, E.A. Nytko, B.M. Bartlett, M.P. Shores, D.G. Nocera, *Phys. Rev. Lett.* **100**, 077203 (2008)
 79. P. Carretta, R. Pasero, M. Giovannini, C. Baines, *Phys. Rev. B* **79**, 020401(R) (2009)
 80. P. Gegenwart, T. Westerkamp, C. Krellner, Y. Tokiwa, S. Paschen, C. Geibel, F. Steglich, E. Abrahams, Q. Si, *Science* **315**, 969 (2007)
 81. Y. Kono, T. Sakakibara, C.P. Aoyama, C. Hotta, M.M. Turnbull, C.P. Landee, Y. Takano *Phys. Rev. Lett.* **114**, 037202 (2015)
 82. Y. Matsumoto, S. Nakatsuji, K. Kuga, Y. Karaki, N. Horie, Y. Shimura, T. Sakakibara, A.H. Nevidomskyy, P. Coleman, *Science* **331**, 316 (2011)
 83. J. Dalibard, F. Gerbier, G. Juzeliunas, P. Öhberg, *Rev. Mod. Phys.* **83**, 1523 (2011)
 84. I.B. Spielman, *Ann. Rev. Cold At. Mol.* **1**, 145 (2012)
 85. H. Zhai, *Int. J. Mod. Phys. B* **26**, 1230001 (2012)
 86. V. Galitski, I.B. Spielman, *Nature* **494**, 49 (2013)

87. X. Zhou, Y. Li, Z. Cai, C. Wu, J. Phys. B: At. Mol. Opt. Phys. **46**, 134001 (2013)
88. N. Goldman, G. Juzeliunas, P. Öhberg, I. B. Spielman, Rep. Progr. Phys. **77**, 126401 (2014)
89. P. Wang, Z.-Q. Yu, Z. Fu, J. Miao, L. Huang, S. Chai, H. Zhai, J. Zhang, Phys. Rev. Lett. **109**, 095301 (2012)
90. L.W. Cheuk, A.T. Sommer, Z. Hadzibabic, T. Yefsah, W.S. Bakr, M.W. Zwierlein, Phys. Rev. Lett. **109**, 095302 (2012)
91. L. Huang, Z. Meng, P. Wang, P. Peng, S.-L. Zhang, L. Chen, D. Li, Q. Zhou, J. Zhang, Nat. Phys. **12**, 540 (2016)
92. G.-B. Jo, Y.-R. Lee, J.-H. Choi, C.A. Christensen, T.H. Kim, J.H. Thywissen, D.E. Pritchard, W. Ketterle, Science **325**, 1521 (2009)
93. R.A. Duine, M. Polini, H.T.C. Stoof, G. Vignale, Phys. Rev. Lett. **104**, 220403 (2010)
94. D. Lidsky, J. Shiraishi et al., Phys. Rev. B, **57**, 1340 (1998)
95. V.A. Khodel, M.V. Zverev, V.M. Yakovenko, Phys. Rev. Lett. **95**, 236402 (2005)
96. D. Yudin, D. Hirschmeier, H. Hafermann, O. Eriksson, A.I. Lichtenstein, M.I. Katsnelson, Phys. Rev. Lett. **112**, 070403 (2014)
97. E.M. Lifshits, L.P. Pitaevsky, Statistical Physics, Part II (Pergamon Press, Oxford, 1980)
98. G.E. Volovik, JETP Lett. **53**, 222 (1991)
99. G.E. Volovik, Acta Phys. Slov. **56**, 49 (2006)
100. G.E. Volovik, in *Quantum analogues: From Phase Transitions to Black Holes and Cosmology*, eds. W.G. Unruh, R. Schutzhold. Springer Lecture Notes in Physics, vol. 718 (Springer, Orlando, 2007), p.31
101. V.R. Shaginyan, JETP Lett. **77**, 99 (2003)
102. V.R. Shaginyan, A.Z. Msezane, V.A. Stephanovich, E.V. Kirichenko, Europhys. Lett. **76**, 898 (2006)
103. V.R. Shaginyan, K.G. Popov, V.A. Stephanovich, E.V. Kirichenko, Journal of Alloys and Compounds **442**, 29 (2007)
104. V.R. Shaginyan, G.S. Japaridze, M.Ya. Amusia, A.Z. Msezane, K.G. Popov, Europhys. Lett. **94**, 69001 (2011)
105. A.J. Leggett, J. Stat. Phys. **93**, 927 (1998)
106. J.I. Božović, X. He, J. Wu, A.T. Bollinger, Nature **536**, 309 (2016)
107. J. Zaanen, Nature **536**, 282 (2016)
108. Y.J. Uemura *et al.*, Phys. Rev. Lett. **62**, 2317 (1989)
109. Y.J. Uemura, A. Keren, L.P. Le, G.M. Luke, W.D. Wu, Y. Kubo, T. Manako, Y. Shimakawa, M. Subramanian, J.L. Cobb, J. T. Markert, Nature **364**, 605 (1993)
110. C. Bernhard, Ch. Niedermayer, U. Binniger, A. Hofer, Ch. Wenger, J.L. Tallon, G.V.M. Williams, E.J. Ansaldo, J.I. Budnick, C.E. Stronach, D.R. Noakes, M.A. Blankson-Mills, Phys. Rev. B **52**, 10488 (1995)
111. P.M.C. Rourke, I. Mouzopoulou, X. Xu, Ch. Panagopoulos, Y. Wang, B. Vignolle, C. Proust, E.V. Kurganova, U. Zeitler, Y. Tanabe, T. Adachi, Y. Koike, N.E. Hussey, Nat. Phys. **7**, 455 (2011)
112. J. Bardeen, L.N. Cooper, J.R. Schrieffer, Phys. Rev. **106**, 162 (1957)
113. G. E. Volovik, Phys. Scr. **T164**, 014014 (2015)

-
114. V.A. Khodel, V.R. Shaginyan, V.V. Khodel, Phys. Rep. **249**, 1 (1994)
 115. A.A. Abrikosov, J.C. Campuzano, K. Gofron, Physica C **214**, 73 (1993)
 116. K. Jin, N.P. Butch, K. Kirshenbaum, J. Paglione, R.L. Greene, Nature, **476**, 73 (2011)
 117. V.A. Khodel, J.W. Clark, K.G. Popov, V.R. Shaginyan, JETP Lett. **101**, 413 (2015)
 118. I.M. Lifshitz, Sov. Phys. JETP **11**, 1130 (1960)
 119. A.A. Abrikosov, L.P. Gor'kov, I.E. Dzyaloshinski, *Methods of Quantum Field Theory in Statistical Physics*, (Dover, New York, 1975)
 120. V.R. Shaginyan, A.Z. Msezane, K.G. Popov, J.W. Clark, M.V. Zverev, V.A. Khodel, Phys. Rev. B **86**, 085147 (2012)